Clays and Clay Minerals, Vol. 68, No. 4:373–393, 2020

EFFECT OF ALKALI CONCENTRATION ON SWELLING CHARACTERISTICS OF TRANSFORMED KAOLINITIC CLAYS

P. L. Sruthi and P. H. P. Reddy*

[1]National Institute of Technology Warangal, Warangal 506004, India

Abstract—Soil–alkali interaction leads to abnormal soil behavior due to significant changes in mineralogy and morphology. The effect of alkali on the swelling behavior of natural clays has been explored in recent years, but the swelling behavior of alkali-transformed clay minerals is still unclear. The objective of the current study was to investigate the effect of alkali concentration on swelling characteristics of natural and alkali-transformed kaolinitic clays. The study was complemented further with micro-level investigations. Red earth and kaolin, which are regarded as non-swelling kaolinitic clays, were utilized. The results showed that alkalis induced greater swelling in natural clays than in alkali-transformed clays. The results revealed further that alkali-transformed clays exhibited decreases in swelling when exposed to increased alkali concentrations. Moreover, the degree of transformation played an important role in the swelling behavior of alkali-transformed kaolinitic clays when inundated with water and with various alkali concentrations. These variations may be attributed to the different extents of mineralogical and microstructural changes caused by alkali treatment.

Keywords—Alkali · Kaolinite · Micro-level investigation · Swelling · Transformed Clay

INTRODUCTION

In modern environments, soil in natural or modified forms has been used increasingly for various civil engineering activities. Directly or indirectly, the effects of modernization and the depletion of natural resources have affected soils adversely due to various anthropogenic activities, including contamination by accidental spills or leakages of industrial effluents (acids, alkalis, etc.), petroleum, heavy metals, and pesticides (Wang 2003; Onojake and Frank 2013). Among the many sources for soil contamination, alkalis are released, for example, from paper, paint, dye, pulp, and aluminum industries and cotton mills.

Alkali contamination has led to soil structural failures due to the formation of neogenic hydrated salts (Sokolovich and Troitskii 1976; Kabanov et al. 1977; Shekhtman et al. 1995). Much research has been conducted to understand the mineral alterations produced by soil/alkali interactions (Cuadros and Linares 1996; Taubald et al. 2000; Wang and Siu 2006a, 2006b; Elert et al. 2008; Jiang et al. 2008; Alshaaer 2013; Elert et al. 2015; Boussen et al. 2015). Continuous wetting of soils by alkalis and exposure of rock-forming minerals to alkaline solutions can lead to neogenic zeolite formation, with the type of zeolite produced depending heavily on the origin, duration of reaction, temperature, and chemistry of the pore fluids. Batch reactor experiments were conducted (Chermak 1992) to understand changes in the mineralogy of the Opalinus shale due to the influence of highly concentrated NaOH solutions. The general sequence of reaction products observed under these high-pH conditions includes the formation of analcime, followed by vermiculite and Na-rectorite. The transformation of montmorillonite into tectosilicates (zeolite) when the pH goes beyond moderately alkaline conditions was reported by Barrer (1982). The formation of zeolites by kaolin–alkali interactions has also been observed (Madani et al. 1990; Akokelar et al. 1997; Demortier et al. 1999). The transformation of saponite to nontronite took place in black cotton soils upon interaction with NaOH (Sivapullaiah et al. 2010). From the above studies, alkali contamination clearly affects the mineralogy of soils, irrespective of the type of mineral (kaolinite/montmorillonite/mixed-layer), and thus may alter soil behavior, including clay-water interactions or swelling.

Mineral–fluid interactions dominate the geotechnical behavior of clayey soils during contamination. The intensity of interaction depends primarily on the nature and quantity of clay minerals and the type and concentration of pore fluids more than on the chemical composition of the soil. Many researchers emphasized the ill effects of caustic soda on the geotechnical features of soils (Maltsev 1998; Jozefaciuk 2002; Reddy et al. 2017). According to Mohnot et al. (1987), mineral loss due to alkalinity is greatest for kaolinite due to soil/alkali reactions and was dominated by chemical reactions. Two of the reactions reported are

$$\underset{\text{(Kaolinite)}}{Al_2Si_2O_5(OH)_4} + 2Na^+ + OH^- + \underset{\text{(Dissolved Silica)}}{4Si(OH)_4} \rightarrow \underset{\text{Na–Feldspar}}{2NaAlSi_3O_8} + 11H_2O \quad (1)$$

$$\underset{\text{(Kaolinite)}}{Al_2Si_2O_5(OH)_4} + 2Na^+ + OH^- + \underset{\text{(Dissolved Silica)}}{2Si(OH)_4} \rightarrow \underset{\text{Analcime}}{2NaAlSi_2O_6.H_2O} + 5H_2O \quad (2)$$

Kaolinite dissolves in alkaline environments and releases alumina and silica monomers, which, upon interaction with NaOH, precipitate as a Na_2O-Al_2O_3-SiO_2-H_2O gel or a zeolite

* E-mail address of corresponding author: hari@nitw.ac.in
DOI: 10.1007/s42860-020-00081-x

Electronic supplementary material The online version of this article (https://doi.org/10.1007/s42860-020-00081-x) contains supplementary material, which is available to authorized users.

(Khajavi et al. 2007; Smith 2009; Samal et al. 2013; Liu and Naidu 2014). Reddy and Sivapullaiah (2010a) discussed the effect of varying NaOH concentrations (1 M, 2 M, and 4 M) on the swelling behavior of three soils with different mineralogies: Black cotton soil predominantly containing montmorillonite, Black cotton soil predominantly containing mixed layer illite-smectite, and red earth predominantly containing kaolinite. Results reported that swelling tendency and neogenic formations in soil with montmorillonite were unaffected by the concentration of NaOH solution, whereas in soil with mixed-layer illite-smectite and soil with kaolinite the swelling increased with increase in concentration, which is mainly due to the formation of sodalites (sodium aluminium silicate hydroxide hydrate). Furthermore, the nature of swelling in soil with mixed-layer illite-smectite varied with concentration, whereas more rapid mineralogical changes were noticed in soil with kaolinite. In a continuation of the above-mentioned work, mineralogical and morphological studies were carried out (Reddy and Sivapullaiah 2010b) in three soils with different mineralogies. Recently, Chavali et al. (2016) observed greater swelling in all three kaolinitic clays with alkali solutions when compared with water. The magnitude of alkali-induced swelling observed in these clays is attributed to dispersion of clay particles and new mineral formations. Thus, micro-level investigations play a predominant role in understanding the swelling behavior of alkali-contaminated soils. In order to mimic the long-term effect of a given alkali concentration on kaolinite mineralogy and microstructure, Sruthi and Reddy (2017) treated kaolinite with various amounts of NaOH, and found significant dissolution of the original kaolinite and precipitation of a new mineral phase, sodalite, thus demonstrating the nature of the effect of alkali on the kaolinite. Still unknown, however, is the effect of alkali exposure and treatment on clay swelling and at which alkali concentrations the greatest effect occurs.

The concentrations of the alkali solutions used in the relevant industries can reach as high as 10 N, and when they leak into the moist ground they become diluted to concentrations ranging from 1 to 4 N (Sivapullaiah and Reddy 2009). According to Mitchell (1993) and Mulyukov (2008), even a 0.1 N alkali solution could alter soil structure. The objective of the present investigation, therefore, was to examine the influence of kaolinite content and concentration of alkali on the swelling behavior and dissolution of existing minerals and on the formation of new minerals in contaminated soils by performing a set of laboratory studies on normal and alkali-transformed kaolinitic clays, and to examine the mineralogical changes and microstructural variations.

MATERIALS AND METHODS

Clays Used

Two clays, red earth (R) and kaolin (K) with kaolinite as the predominant mineral in various proportions, were used in the study. Naturally available red earth was collected from a depth of 1 m from the ground surface in Warangal, Telangana, India, and commercial kaolin was obtained from Godavari mines and minerals, Vizag, A.P, India. Both clays were air-dried and passed through an IS 425 μm sieve. The physical properties (Table 1) and chemical compositions (Table 2) of the clays were determined.

Solutions Used

Four different concentrations (0.1, 1, 4, and 8 N) of sodium hydroxide (NaOH) solution were prepared as per standard procedures (Standard Methods, 2017) by dissolving the required mass of AnalaR-Grade NaOH pellets (S D-Fine Chem Ltd., Mumbai, India) in distilled water.

Experimental Investigation

To bring out the effect of various concentrations of alkali (NaOH) solutions on mineral dissolution of kaolinitic clays and the formation of new minerals, experiments were performed under specific conditions that simulate long-term effects of alkali on the samples. The experimental procedure mentioned by Sruthi and Reddy (2017) was adopted. Initially, raw clay samples were mixed using smaller volumes of interacting solution (4 N was used because most industrial contamination is close to this value), i.e. 1× the moisture content at the liquid limit (LL). After a 1-day interaction in a desiccator, samples were dried in the oven at 110°C. The dried samples were pulverized manually into fine powders using a mortar and pestle and passed through a No. 200 sieve (75 μm). The powdered samples were subjected to analysis by X-ray diffraction (XRD). The entire procedure was repeated by mixing raw clay samples with greater volumes of interacting solution. The samples were mixed in batches, i.e. separate samples were prepared for each volume of interaction solution (1, 2.5, 3.5, 5, 6, 7, 8, and 10 × LL moisture content). This procedure was continued until complete dissolution of kaolinite was confirmed by XRD analysis. Based on the procedure mentioned above, the specific conditions selected for the current investigation were: temperature (110°C), volume of interacting solution (7 × LL for R and 10 × LL for K), and duration of interaction (1 day). The samples were allowed to interact with specific concentrations (0.1, 1, 4, and 8 N) of alkali (NaOH) solutions. After interaction with NaOH

Table 1. Physical properties of kaolinitic clays

Properties	Red earth (R)	Kaolin (K)
Specific gravity	2.62	2.70
Liquid limit (LL), (%)	38.0	42.9
Plastic limit (PL), (%)	22.64	29.72
Plasticity index (PI), (%)	15.36	13.18
Free swell index (mL/g)	1.0	1.1
Max. dry unit weight kN/m^3	18.3	17.0
Optimum water content (%)	20.74	27.05
Clay content (%)	26	32
Silt content (%)	38	68
Fine sand content (%)	36	-
Cation exchange capacity (meq/100 g)	9.39	5.62

https://doi.org/10.1007/s42860-020-00081-x Published online by Cambridge University Press

Table 2. Chemical composition of kaolinitic clays

Clay	SiO_2	Al_2O_3	Fe_2O_3	MgO	CaO	Na_2O	K_2O	TiO_2	P_2O_5	MnO	SO_3
R	34.6	29.1	24.6	3.8	3.5	0.2	0.5	2.0	0.22	0.75	0.125
K	32.5	48.80	8.2	2.9	4.6	0.09	0.3	2.2	0.15	0.17	0.11

solutions, the samples were filtered, dried, and allowed to swell after inundation with water and with the respective transformed concentrations (i.e. a 0.1 N transformed sample was inundated with 0.1 N, a 1 N transformed sample with 1 N, and a 4 N transformed sample with 4 N) in oedometer consolidation cells. Swelling studies for the 8 N transformed samples were not performed with water or transformed concentrations because of the difficulty of placing the samples in the oedometer cell. The variations in mineralogy and changes in morphology due to interaction with alkali solutions were analyzed using XRD and scanning electron microscopy (SEM), respectively. Quantification of raw- and transformed-clay minerals was done according to the procedure reported by Garvie and Nicholson (1972) and Mazaheri et al. (2008). Further, Fourier-transform infrared (FTIR) spectroscopy and thermogravimetric-differential thermal analyses (TG-DTA) were performed to reconfirm the mineralogical changes.

One-dimensional Free Swell Tests

One-dimensional free swell tests were carried out on the natural and transformed samples by inundating them in water and NaOH solutions continuously. The one-dimensional free swell test procedure adopted was mentioned by Puppala et al. (2005). The final swell displacements along with the original heights of the soil specimens were used to calculate swell strains in the vertical direction.

Swell (%) in soils is calculated as a percentage ratio of the increase in thickness relative to the original thickness using Eq. 3

$$\varepsilon = \Delta H/H \times 100\% \quad (3)$$

where ε is swell percent, and ΔH and H are the change in thickness and original thickness of the samples, respectively.

After attaining equilibrium, treatments on swollen samples were terminated and the samples were oven dried. Experiments were repeated twice to check the reproducibility of results. Representative soil samples were collected at the completion of the free swell tests, and mineralogical and microstructural investigations were carried out to understand particle-level interactions.

X-ray Diffraction Studies

The XRD patterns were recorded using a PANalytical X'Pert Powder X-ray diffractometer (Almelo, Netherlands) with the help of an X'Celerator ultra-fast detector. The X-ray tube (Ni-filtered CuKα) was operated at 60 kV and 55 mA. The data were collected from 6 to 70°2θ with a step size of 0.01°2θ. The samples were ground manually and a representative sample was pressed gently into glass holders. For qualitative identification of minerals, *X'pert high score plus* software based on the PCPDFWIN database was used.

Scanning Electron Microscopy Studies

The microstructures of the samples were analyzed using TESCAN VEGA 3LMU (Brno, Czech Republic) scanning electron microscopy (SEM). A conventional W heated cathode with 3D beam technology was used. Prior to scanning, a gold coating was sputtered onto the samples

Fourier-Transform Infrared Spectroscopy

The FTIR analysis of the samples was conducted using a Perkin Elmer 100S FTIR spectrophotometer (Shelton, Connecticut, USA) equipped with a standard DTGS detector. Samples were prepared using the KBr pellet method and scanned at a resolution of 4 cm^{-1} over the spectral range 4000 to 400 cm^{-1}.

Differential Thermo-gravimetric Analysis

To determine structural changes and losses in sample mass, differential thermal analysis (DTA) and thermo-gravimetric analysis (TGA) were conducted. The tests were performed using a NETZSCH STA 2500 Regulus thermal analysis instrument (Selb, Germany). Samples were tested at a heating rate of 10°C/min to 1000°C in Ar.

RESULTS

Effect of Various NaOH Concentrations on Swelling Behavior of Alkali-transformed Red Earth

Free swell test results of red earth (R) and alkali-transformed red earth samples (red earth samples transformed with 0.1, 1, and 4 N NaOH are represented as 0.1R, 1R, and 4R, respectively) when inundated with water (represented as R-W, 0.1R-W, 1R-W, and 4R-W) exhibited swelling of ~1%, 3%, 5%, and 8%, respectively (Fig. 1). Further, alkali-transformed red earth samples inundated with the respective transformative concentrations (represented as 0.1R-0.1 N, 1R-1 N, and 4R-4 N) exhibited swelling of ~17%, 14%, and 7.5%, respectively (Fig. 1a–c). To explain the variations in the swell behavior of transformative samples, the results were compared to the natural, non-transformed samples. The mineralogical alterations, which took place during swelling, were identified using XRD analyses of all samples.

XRD Analyses of Red Earth Samples Before and After Swelling

The XRD pattern of red earth (R) shows peaks pertaining to quartz, kaolinite, and hematite (Fig. 2). The red earth sample reacted with 0.1 N NaOH solutions (0.1R) showed no changes in the XRD pattern (Fig. 2a); in 1R, very small traces of sodalite were identified (Fig. 2a). With an increase in the concentration to 4 N (i.e. sample 4R), kaolinite dissolution (7.13 and 4.28 Å) and more intense sodalite peaks appeared (Fig. 2a). Sodalite, which belongs to the zeolite group, forms in

https://doi.org/10.1007/s42860-020-00081-x Published online by Cambridge University Press

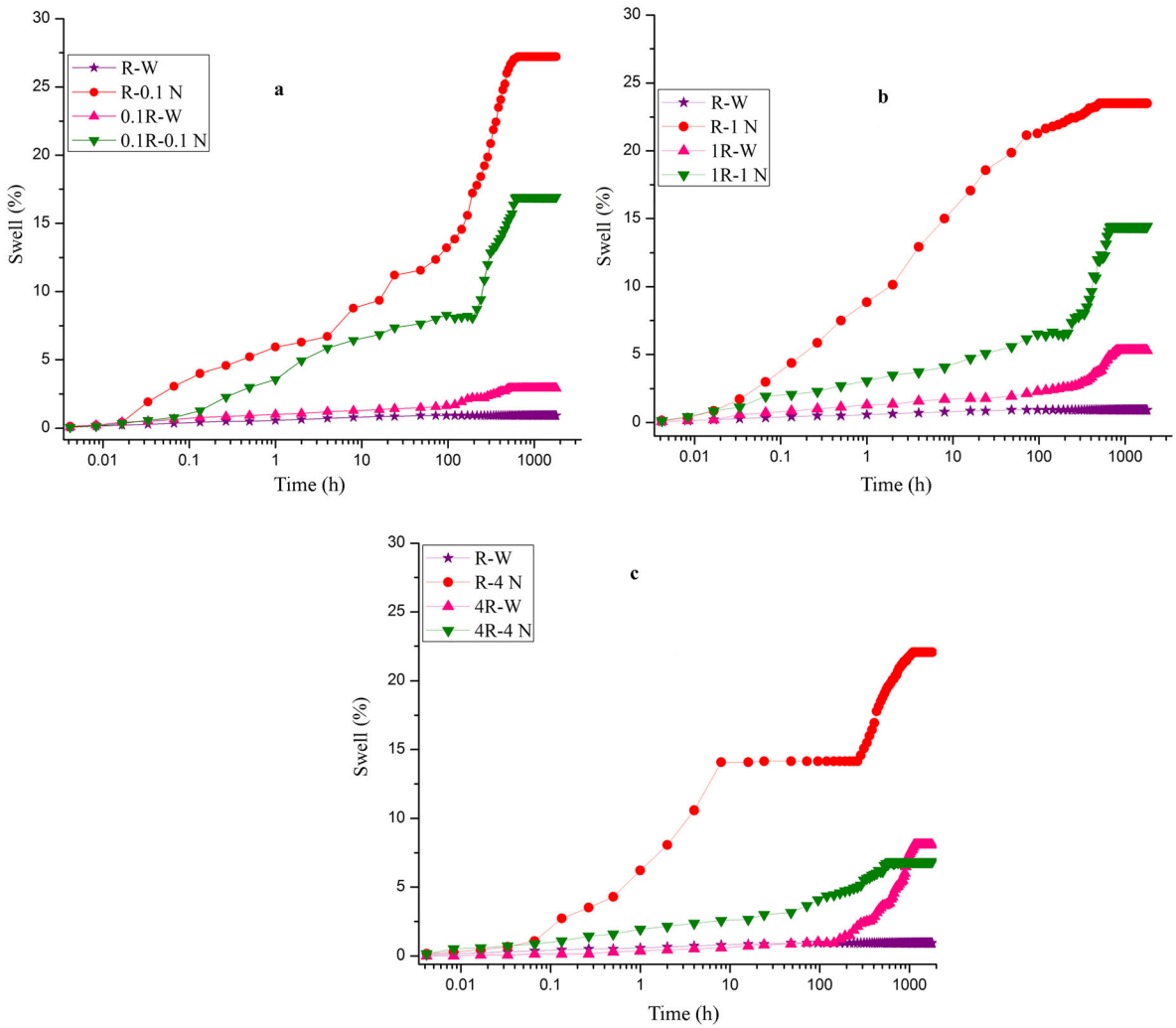

Fig. 1. Swelling behavior of transformed and non-transformed red earth samples inundated with water and alkali solutions

alkaline systems with alumina and silica. Also at 4R, traces of topaz with less intense peaks (Fig. 2a) were noted. With an increase in concentration to 8 N (i.e. sample 8R), in addition to sodalite, new mineral peaks attributed to trona were observed (Fig. 2a). Thus, XRD analysis of red earth samples reacted with various concentrations of NaOH showed complete kaolinite dissolution; new-mineral formation occurred mainly at the higher concentrations, i.e. 4 N and 8 N solutions.

After the swell test, red earth samples (0.1R-0.1 N, 1R-1 N, and 4R-4 N) were subjected to analysis by XRD (Fig. 2b). The XRD pattern of 0.1R-0.1 N showed little variation in mineralogy except for the formation of albite (Fig. 2b); new peaks for flusston (Ayoob et al. 2011; Ogbaji et al. 2018) and sodalite were observed in the 1R-1 N sample (Fig. 2b). The formation of new minerals, however, does not imply complete dissolution of kaolinite in either of the 0.1R-0.1 N and 1R-1 N samples. The XRD patterns of 4R-4 N had more intense sodalite peaks (Figs. 2b and 3b) and evidence of another new mineral, natrite (Figs. 2b, 3b). According to Zubkova et al. (2002), natrite is one of the rarest species of the six in the soda minerals group. Natrite is the only mineral in the group which does not contain hydrogen atoms. This is a peculiarity considering the mineral is an endogenous high-temperature species (Zubkova et al. 2002). Furthermore, in sample 4R-4 N, complete kaolinite dissolution was apparent. Mineral quantification of the red earth samples revealed a variation in the percent mineral contents (Fig. 3a, b) of each mineral identified using XRD (*d* spacings listed in Table 3). Raw XRD data for red earth samples before and after swelling are given in supplementary Table S1.

SEM Studies of Red Earth Samples Before and After Swelling

The morphology of the red earth and the 0.1 to 8 N NaOH-transformed red earth samples was determined by SEM (Fig. 4) and revealed a compacted and aggregated morphology (Fig. 4a). No significant change in morphology was observed in sample 0.1R (Fig. 4b). A micrograph of sample 1R (Fig. 4d) showed traces of reaction products, which was consistent with the XRD analyses. Sample 4R showed a distinct morphology (Fig. 4f) with significant reaction products supplementing the partially dissolved kaolinite and the new mineral peak observed in the

https://doi.org/10.1007/s42860-020-00081-x Published online by Cambridge University Press

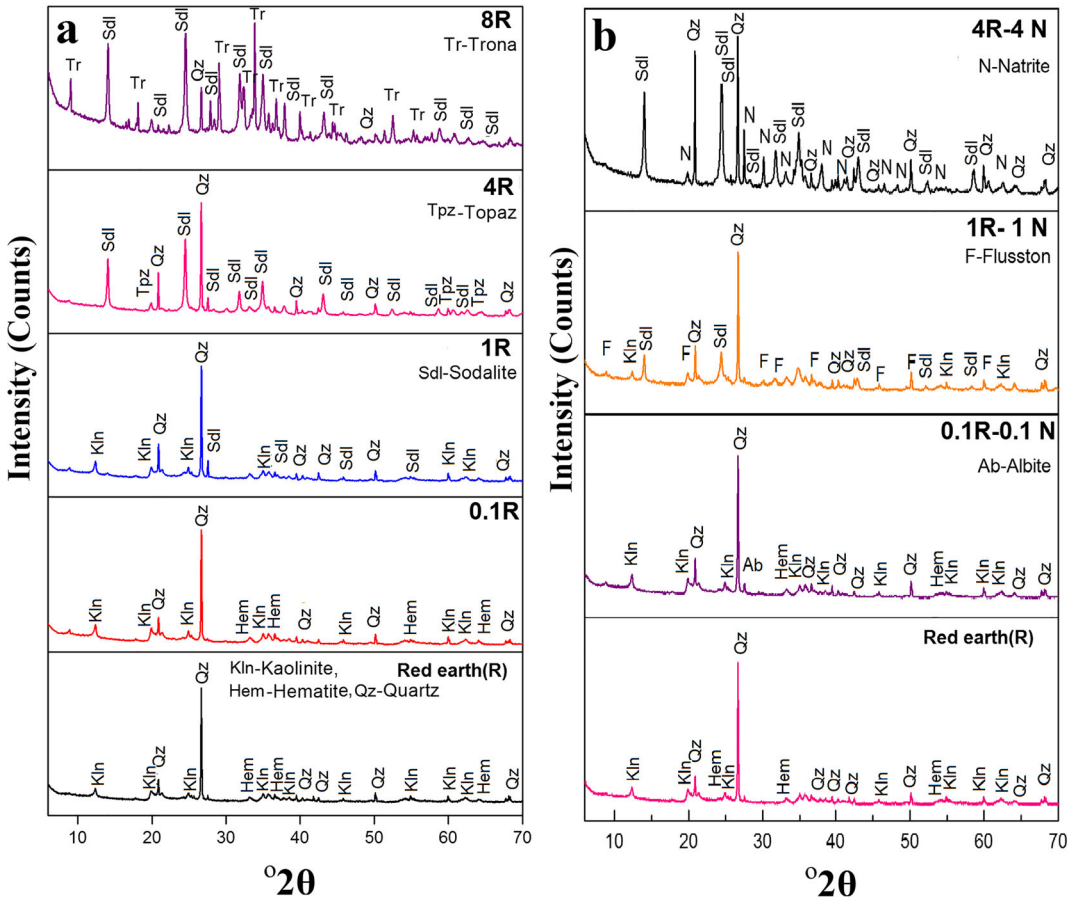

Fig. 2. XRD patterns of red earth **a** before and **b** after swelling tests

XRD analyses. The morphology of topaz varies widely according to its origin and formation. In the present study, particles with morphology typical of topaz (Russell 1924) were observed (Fig. 4f). After an increased interaction with 8 N NaOH, well defined sodalite crystals (Fig. 4h) were formed, corroborating the intense sodalite peaks observed in the XRD analyses of 8R (Fig. 2a). Coalesced pellet formations representing crystalline trona were also observed (Fig. 4h). A micrograph of sample 0.1R-0.1 N (Fig. 4c) showed a weathering-related change in morphology. An SEM image of 1R-1 N (Fig. 4e) also showed weathering and the formation of particles with the distinct crystal morphology of sodalite. Flusston formation was minimal and the particles did not have a clear morphology. The presence of sodalite in the micrograph of 4R-4 N (Fig. 4g) was evident in the form of cotton balls. Natrite appeared as small, isolated, efflorescent growths, which were surrounded by relatively large porous areas (Ball et al. 1986). Face-face association, i.e. parallel orientation of the particles, was clearly visible (Fig. 4g), which supports the more limited swelling observed.

FTIR Analyses of Alkali-transformed Red Earth due to Interaction with Various NaOH Concentrations

The FTIR spectra of sample R and its NaOH transformed products (Fig. 5, Table 4) contained a band at 3696 cm^{-1} and 3621 cm^{-1} indicating OH vibrations of kaolinite. When the red earth reacted with 0.1 N NaOH (0.1R), no significant alterations in bands were observed, which indicates no new minerals were formed (Fig. 5a). However, a peak at 1008 cm^{-1} in the 0.1R sample might be due to quartz interference (Si–O) (Diko et al. 2016). For the R sample treated with 1 N NaOH (1R), the intensity of the 912 cm^{-1} band decreased, which indicates kaolinite disintegration and the 1414 cm^{-1} band indicated a small number of carbonate groups. For the 4 N (4R) and 8 N (8R) NaOH-treated R samples, remarkable changes were noticed in the FTIR spectra (Fig. 5a). The wide band observed from 3400–3700 cm^{-1} (centered at 3464 cm^{-1} in 4 N (4R) and 3459 cm^{-1} in 8 N (8R)) was assigned to stretching of water molecules adsorbed on sodalite OH groups (Schnabel et al. 1997; Popescu et al. 2001; Ren et al. 2003; Esfandian et al. 2016). The development of peaks around 1452 cm^{-1} and 1451 cm^{-1} in the 4R and 8R samples, respectively, are usually ascribed to three-fold coordinated Al (Kamseu et al. 2016). For the R sample treated with 8 N NaOH, a new peak in the 8R sample at 864 cm^{-1} was attributed to carbonate ion vibrations (Blanco et al. 2011). The presence of carbonates in trona was indicated by a band at 864 cm^{-1}. FTIR spectra of 0.1R-0.1 N and 1R-1 N (Fig. 5b) showed little variation in the spectra when compared to 0.1R and 1R, respectively. The FTIR spectra of 4R-4 N showed slight variations compared to 4R, however, in terms of the

https://doi.org/10.1007/s42860-020-00081-x Published online by Cambridge University Press

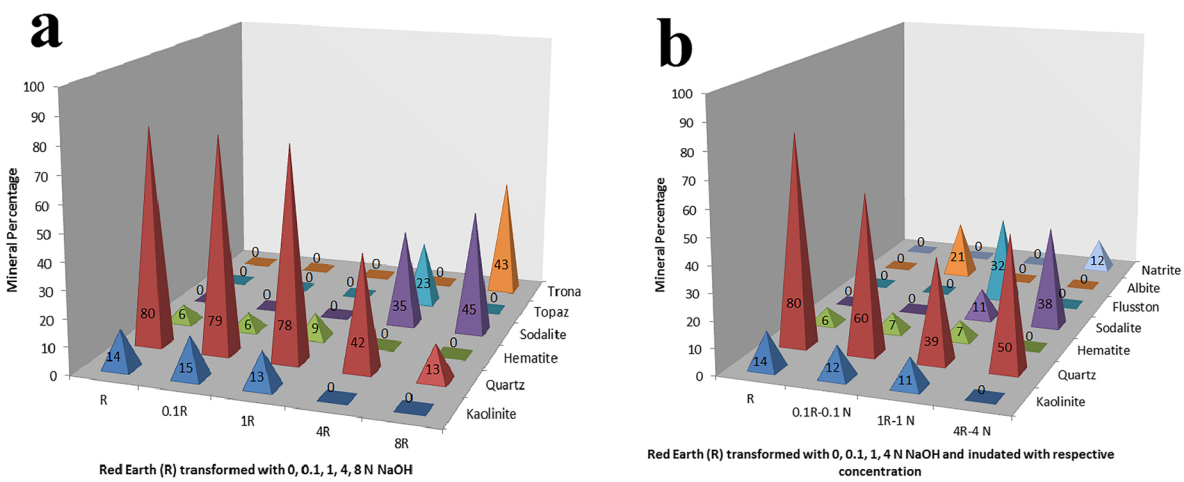

Fig. 3. Mineral quantification of transformed red earth **a** before and **b** after swelling tests

disappearance of bands at 734 and 707 cm^{-1} (Fig. 5b). Raw FTIR data for red earth samples before and after swelling are given in supplementary Table S2.

Thermogravimetric Analyses of Alkali-transformed Red Earth

The DTA curve of sample R (Fig. 6a) had endothermic peaks at 74, 491, and 574°C and an exothermic peak at 938°C, which are characteristic features of kaolinite minerals. The peak at 74°C indicated that the hygroscopic water content was small, whereas peaks at 491 and 574°C indicated deoxydrilation (Deoxydrilation of clay minerals refers to the loss of an interbedded hydroxyl, which occurs over a wide temperature range, 300–700°C; Amadori et al., 2018) and dehydroxylation of kaolinite. The exothermic peak at 938°C was ascribed to the formation of a new-mineral crystalline phase.

The endothermic peaks at 75°C and 94°C in the 0.1R and 1R samples, respectively, were due mainly to the loss of hygroscopic water (Fig. 6b). The second endothermic peaks at 491°C (0.1R) and 471°C (1R) shifted to lower temperatures and indicated that minerals in sample R were degraded to a certain degree. This indicated that the red earth sample was affected by the 0.1 N and 1 N NaOH alkali solutions. The DTA curve of 4R showed a strong and sharp endothermic peak at 104°C (Fig. 6a), which was mainly due to loss of water molecules from zeolite cavities. The endothermic peak at 636°C corresponds to sodalite decomposition. In the temperature range 50–300°C, the zeolite minerals had a characteristic endothermic peak due to desorption of water. This might be the reason for the endothermic peaks at 104 and 213°C in 4R and 8R samples, respectively.

The DTA curve of the 0.1R-0.1 N and 1R-1 N samples had endothermic peaks at 85 and 100°C (Fig. 7a), which were mainly due to the loss of hygroscopic water. The second endothermic peak at 491°C (Fig. 7a) in 0.1R-0.1 N showed that minerals present in the sample were degraded to some extent. The DTA curve of 4R-4 N showed a sharp

Table 3. Diagnosed *d* spacing values of soil alkali reaction products formed

Notation	Mineral	Major diagnosed *d* spacings	Chemical formula
Kln	Kaolinite	7.20A (001), 4.450A (002), 3.59A (003)	$Al_2Si_2O_5(OH)_4$
Qz	Quartz	3.34A (001), 4.25A (002), 1.81A (003)	SiO_2
Hem	Hematite	2.69A (001), 2.51 (002)	Fe_2O_3
Cal	Calcite	3.03A (001), 1.87A (002), 3.87A (003)	$CaCO_3$
Soil-NaOH reaction products			
Sdl	Sodalite	6.30A (001), 3.62A (002), 2.80A (003)	$Na_8Al_6Si_6O_{24}$ (OH)$_2$ (H_2O)$_2$
Tpz	Topaz	3.24A (001), 2.96 (002)	$Al_2(SiO_4)(OH)_2$
Tr	Trona	2.64A (001), 3.07A (002), 9.79A (003)	$Na_3H(CO_3)_2$ $(H_2O)_2$
Ab	Albite	3.23A (001), 4.85A (003)	$Na(AlSi_3O_8)$
N	Natrite	2.96A (001), 2.36A (002),2.17A (004)	Na_2CO_3
Anl	Analcime	3.43A (001), 4.85A (003)	$Na(AlSi_2O_6)(H_2O)$
Zeo X	Zeolite X	14.49(001)	$Na_{92.8}$ ($Al_{88}Si_{104}O_{384}$)
F	Flusston	4.46(002), 2.58(003)	SiO_2-Al_2O_3- Na-OH

https://doi.org/10.1007/s42860-020-00081-x Published online by Cambridge University Press

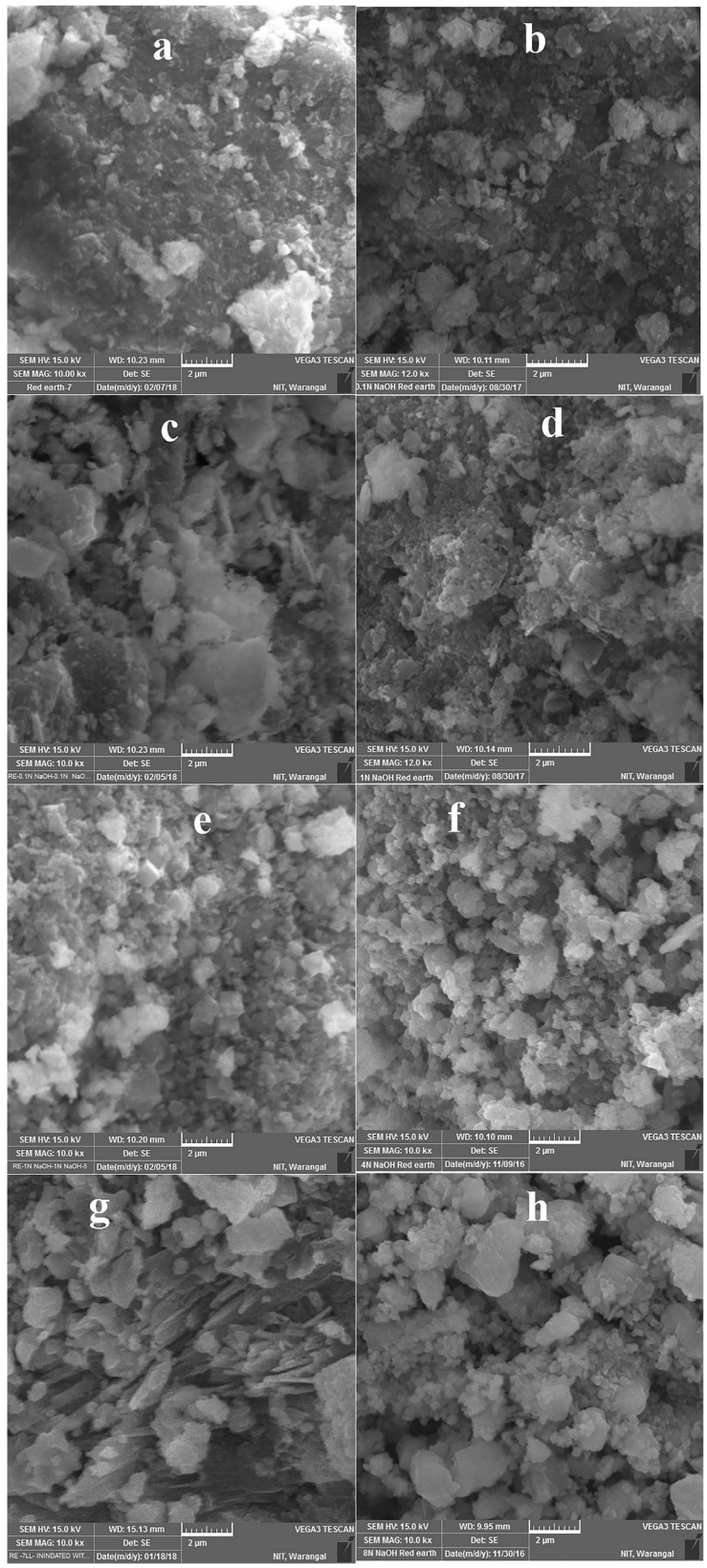

Fig. 4. SEM images of samples **a** red earth (R), **b** 0.1R, **d** 1R, **f** 4R, and **h** 8R interacted with water; **c** 0.1R-0.1 N, **e** 1R-1 N, and **g** 4R-4 N. Scale bars = 2 µm

https://doi.org/10.1007/s42860-020-00081-x Published online by Cambridge University Press

Table 4. Assignments and infrared band positions of sample R and transformed R samples inundated with varying concentrations of NaOH solution

Sample no	Position (cm^{-1}) from previous studies	R	0.1R	1R	4R	8R	0.1R-0.1 N	1R-1 N	4R-4 N	Assignments
1	3696, 3621	3696, 3621	3696, 3620	3695, 3620	------	------	3695, 3650,3620	3696, 3620	-----	-OH stretching
2	3445	3434	3435	3435	3464	-------	3451	3465	3465	Al–O-H stretching (physisorbed water)
3	2924	2924	------	------	------	------	------	------	------	C–H stretching
6	1632	1631	1637	1642	1652	1658	1634	1654	1683	-OH bending, hydration
7	1426	1407	------	1414	1452	1451	------	1476	1452,1410	CO_3 stretching of calcite
8	1032, 1008	1034	1033, 1008	1032, 1008	987	1008	1033, 1008	1030, 1007	993	Si–O stretching, in-plane/ Si-O-Si stretching (Frost et al. 2004)
9	913	913	912	912	------	------	912	----	-----	Al-OH bending
10	864	-----	-----	-----	-----	864	----	----	866,849,	Carbonate ion vibrations (Blanco et al. 2011)
11	798	797	796	797	798	------	796	797	797	OH deformation linked to Al^{3-}
12	750-670	-----	-----	-----	734,707	-----	-----	-----	----	Presence of zeolites/ Si–O–Al str
13	696	695	695	694	------	-----	694	693	----	Si–O stretching, out-of-plane
14		-----			664	658		658	656	*Alumino silicates
15	538	539	538	538	537	540	538	537	596	*Fe–O, Fe_2O_3; Si–O–Al stretching
16	475-68	471	470	470	465	467	470	469	461	Si-O-Si bending
17	430	434	431	-----	434	-----	430	430	431	Si–O deformation/ Al–O Stretching band (Farmer, 1974)

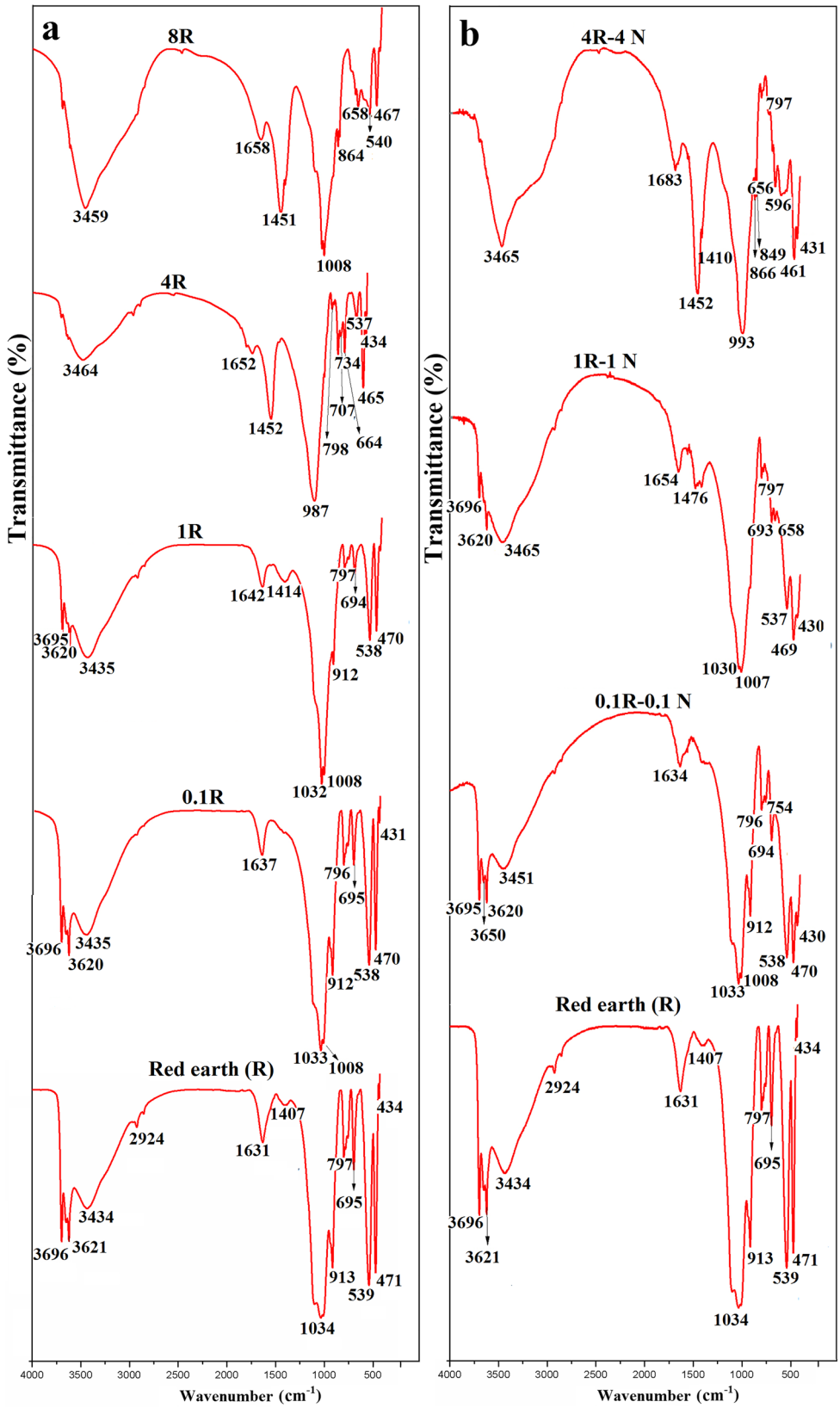

Fig. 5. FTIR spectra of **a** red earth and **b** alkali-transformed red earth interacted with various NaOH concentrations

https://doi.org/10.1007/s42860-020-00081-x Published online by Cambridge University Press

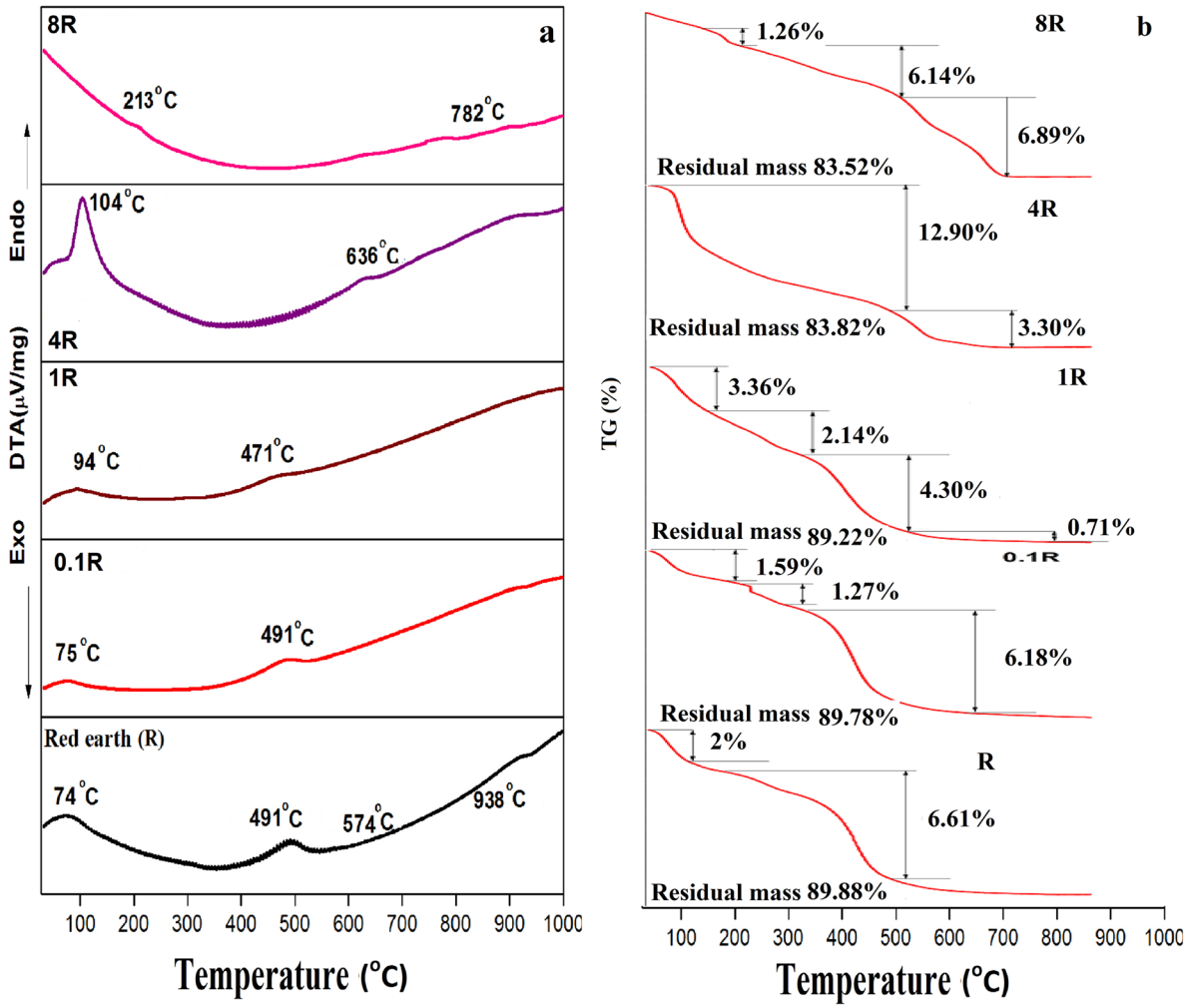

Fig. 6. a DTA and **b** TG curves of red earth interacted with various NaOH concentrations

endothermic peak at 212°C (Fig. 7a), which was mainly due to the loss of water molecules from zeolite cavities. Mass losses corresponding to endothermic peaks were identified (Fig. 7b). In the 0.1R-0.1 N, 1R-1 N, and 4R-4 N samples, the endothermic peak at 574°C was absent and indicated kaolinite dissolution.

Effect of Various NaOH Concentrations on Swelling Behavior of Alkali-transformed Kaolin

The free swell tests on kaolin (K) samples (kaolin samples transformed with 0.1, 1, and 4 N NaOH are designated 0.1K, 1K, and 4K) inundated with water and NaOH solutions are presented in Fig. 8. The kaolin samples inundated with water are hereafter designated K-W, 0.1K-W, 1K-W, and 4K-W; the kaolin samples inundated with 0.1 N, 1 N, and 4 N NaOH solutions are hereafter designated 0.1K-0.1 N, 1K-1 N, and 4K-4 N, respectively. Transformed samples (0.1K-W, 1K-W, and 4K-W) exhibited swelling of ~4.5, 7, and 11% (Fig. 8a, b, c), respectively, compared to non-transformed samples (K-W). On the other hand, the 0.1K-0.1 N, 1K-1 N and 4K-4 N samples exhibited swelling of ~8.5, 7.78, and 7.92%, respectively (Fig. 8a, b, c).

Kaolin (K) had very limited swelling and exhibited only 3% swelling when inundated with water. Upon inundation with 0.1 N, 1 N, and 4 N NaOH solutions, kaolin exhibited swelling of ~16% (K-0.1 N), 12% (K-1 N), and 22% (K-4 N), respectively, as reported by Chavali et al. (2016).

XRD Analyses of Kaolin Samples Before and After Swelling

The XRD patterns of kaolin showed peaks due to quartz, kaolinite, and calcite (Fig. 9a). No changes in XRD pattern were observed for sample 0.1K. In the 1K sample, less intense sodalite peaks were observed and the calcite peak remained unaltered. In the 4K sample, a drastic reduction in the intensity of kaolinite peaks with a simultaneous increase in the intensity of sodalite peaks was noticed and the calcite peak disappeared completely. Differences in the quantity of minerals in the samples were revealed (Fig. 10a). A reduction in the intensity of the kaolinite peaks marked the disintegration of the mineral, which liberated silica and alumina and formed sodalite. Besides sodalite peak formation, new, less intense natrite peaks appeared. Complete dissolution of calcite might explain the formation of natrite.

https://doi.org/10.1007/s42860-020-00081-x Published online by Cambridge University Press

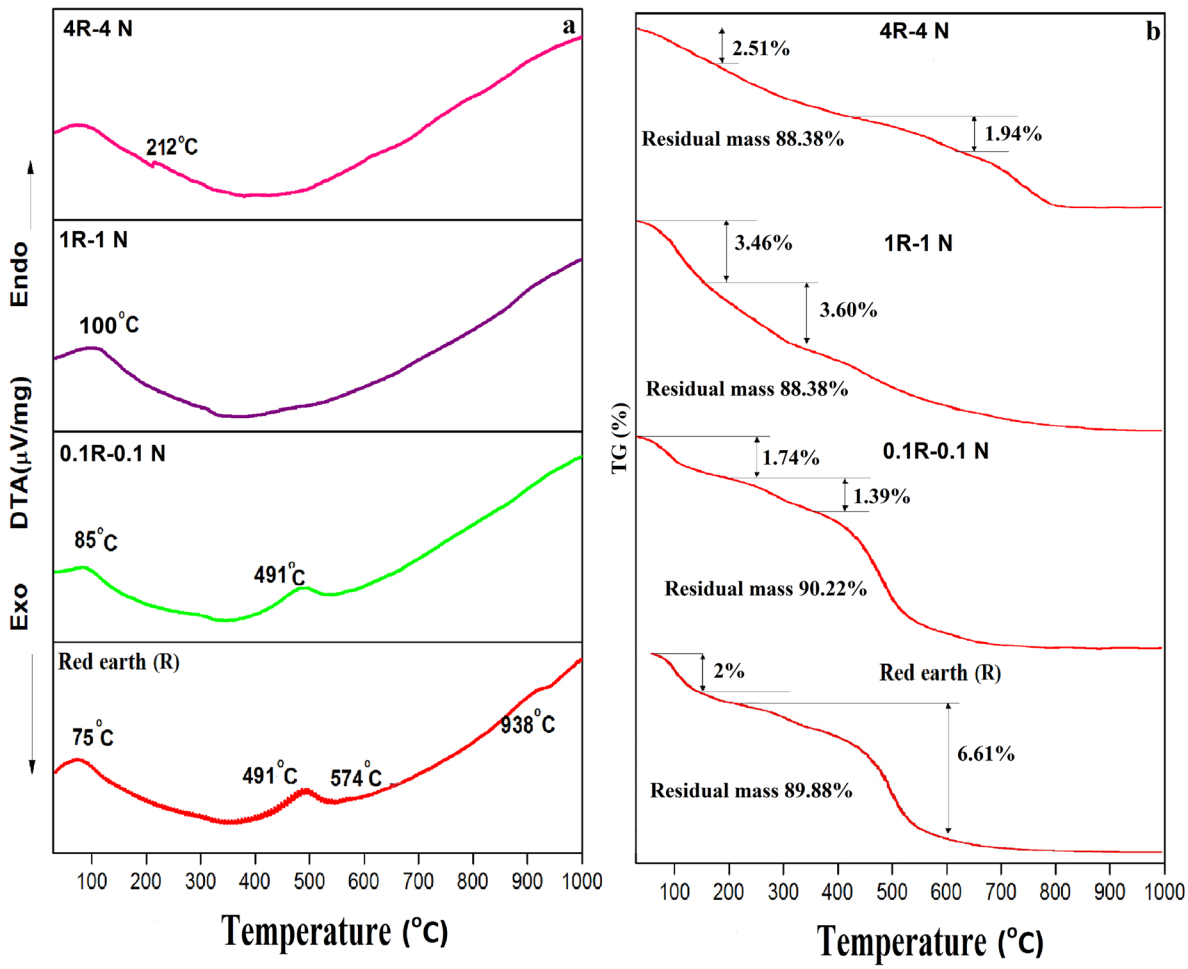

Fig. 7. a DTA and **b** TG curves of alkali-transformed red earth, interacted with various NaOH concentrations

With an increase in NaOH concentration to 8 N, a tremendous increase in the intensity of sodalite and natrite peaks was noticed (Figs. 9, 10a). Besides sodalite and natrite, new analcime peaks were also observed. Johnson and Arshad (2014) reported the formation of sodalite and analcime (sodium aluminum silicate hydrate) at greater concentrations of NaOH (3.99 M). The XRD data indicated that kaolinite dissolution and new-mineral formation occurred mainly in the 4 N and 8 N NaOH solutions. The XRD pattern of 0.1K-0.1 N revealed the formation of zeolite X (Figs. 9b, 10b). Zeolite X is a sodium aluminum silicate mineral formed due to dissolution of silica and alumina from kaolinite. The XRD pattern of 1K-1 N (Fig. 9b) showed an increase in the sodalite peak intensities (refer to Fig. 10b for quantification of sodalite) and the XRD pattern of 4K-4 N (Fig. 9b) showed a tremendous increase in the intensity of the sodalite peaks (Fig. 10b) which corresponded to complete dissolution of kaolinite. The *d* spacing of the minerals identified from the XRD analysis of the kaolin samples are listed in Table 3. Raw XRD data for kaolin samples before and after swelling are given in supplementary Table S3.

SEM Studies of Kaolin Samples Before and After Swelling

The SEM studies illustrated the effects of various NaOH concentrations (0.1 to 8 N) on the morphology of kaolin particles (Fig. 11). An SEM image of kaolin showed a loose fibrous structure (Sruthi and Reddy 2017). An SEM image of 0.1K showed only a subtle change in morphology (Fig. 11b), which was difficult to differentiate and interpret from the existing images. The SEM image of the 1K (Fig. 11d) sample highlighted the formation of trace amounts of sodalite and had a cotton-ball like morphology (Barnes et al. 1999). Severe morphological changes were observed in the 4K sample (Fig. 11f) with the formation of distinct sodalite particles and indicated an increase in the size of sodalite particles. In the 8K sample, a complete grouping of sodalite particles took place with layered structures on the surface of grouped sodalite particles (Fig. 11h). Small traces of analcime particles showed indistinct octahedral and tetrahedral crystal morphologies (Ibrahim 2004) (Fig. 11h). The weathering of a swollen sample (0.1R-0.1 N) is clearly visible in Fig. 11c. Tiny groups of particles with a cotton ball-like morphology supported the idea of formation of sodalite (Fig. 11e) as confirmed by XRD analysis. The micrographs of the 4K-4 N sample (Fig. 11g)

https://doi.org/10.1007/s42860-020-00081-x Published online by Cambridge University Press

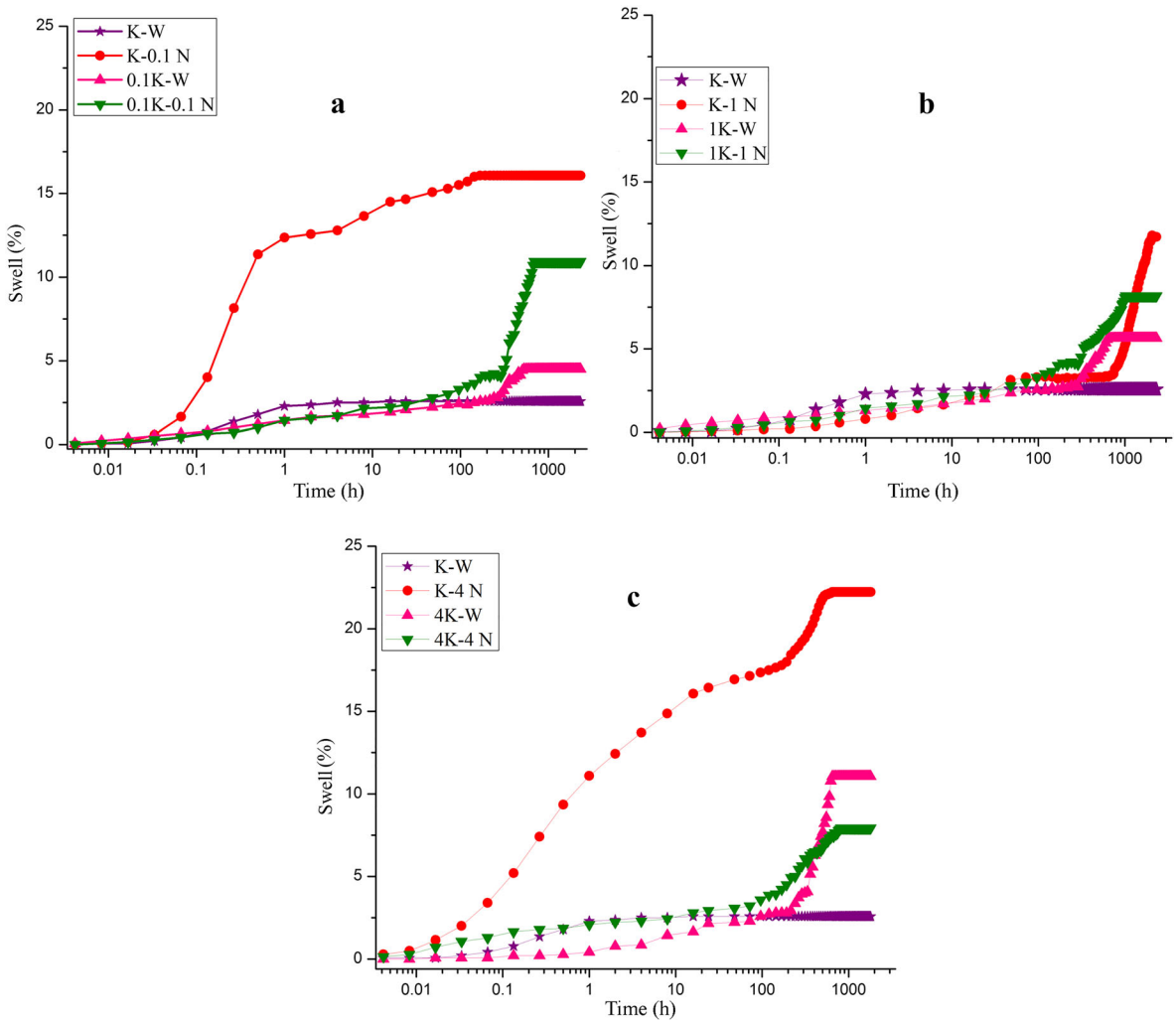

Fig. 8. Swelling behavior of transformed and non-transformed kaolin samples inundated with water and alkali solutions

had distinctly grouped formations of particles with a cotton-ball-like morphology with dense packing, which also supports the limited swelling observed in sample 4K-4 N. Fibrous structures seen in kaolin (Fig. 11a) were completely absent from the 4K (Fig. 11f), 4K-4 N (Fig. 11g), and 8K samples (Fig. 11h). Thus, changes in particle morphology provided evidence for mineralogical alterations.

In summary, changes in mineralogy and morphology reflected the treatment conditions, i.e. initial mineral content, type and concentration of reacting solution, hydrothermal conditions, and duration of the reaction. Furthermore, FTIR and TG-DTA analyses corroborated the changes in mineralogy and morphology observed by XRD and SEM.

FTIR Analyses of Kaolin Samples Before and After Swelling

The FTIR spectrum of the K sample was similar to that of the R sample with an additional stretching band appearing at 1426 cm^{-1}, which indicated the presence of calcite (Fig. 12; Table 5). Weak bands at 2924 cm^{-1} and 2494 cm^{-1} appeared in the carbonyl region for the 4 N NaOH samples (Fig. 12a). The characteristic sodalite absorption bands at 978 cm^{-1} (4K) and 983 cm^{-1} (8K) were attributed to asymmetric atomic vibrations (Vaiciukyniene et al. 2009). A band at 912 cm^{-1}, which is characteristic of kaolinite, was absent from both the 4 N and 8 N NaOH-treated samples which highlights the dissolution of kaolinite at higher NaOH concentrations (Table 5).

The FTIR spectra of 0.1K-0.1 N and 1K-1 N (Fig. 12b) showed little variation compared with those of 0.1K and 1K. The FTIR spectrum of 4K-4 N showed a slight variation in comparison to 4K, however, in terms of the disappearance of the bands at 2924 and 2494 cm^{-1}. Raw FTIR data for kaolin samples before and after swelling are given in supplementary Table S4.

Thermo-gravimetric Analyses of Alkali-transformed Kaolin

The DTA curve of kaolin with an endothermic peak at 59°C (Fig. 13a) was accompanied by a weight loss of 1.49% (Fig. 13b). An endothermic peak at 525°C was due mainly to dehydroxylation of the mineral, due to the removal of hydroxyl groups from Al–OH bonds (Rocha and Klinowski 1990). A

https://doi.org/10.1007/s42860-020-00081-x Published online by Cambridge University Press

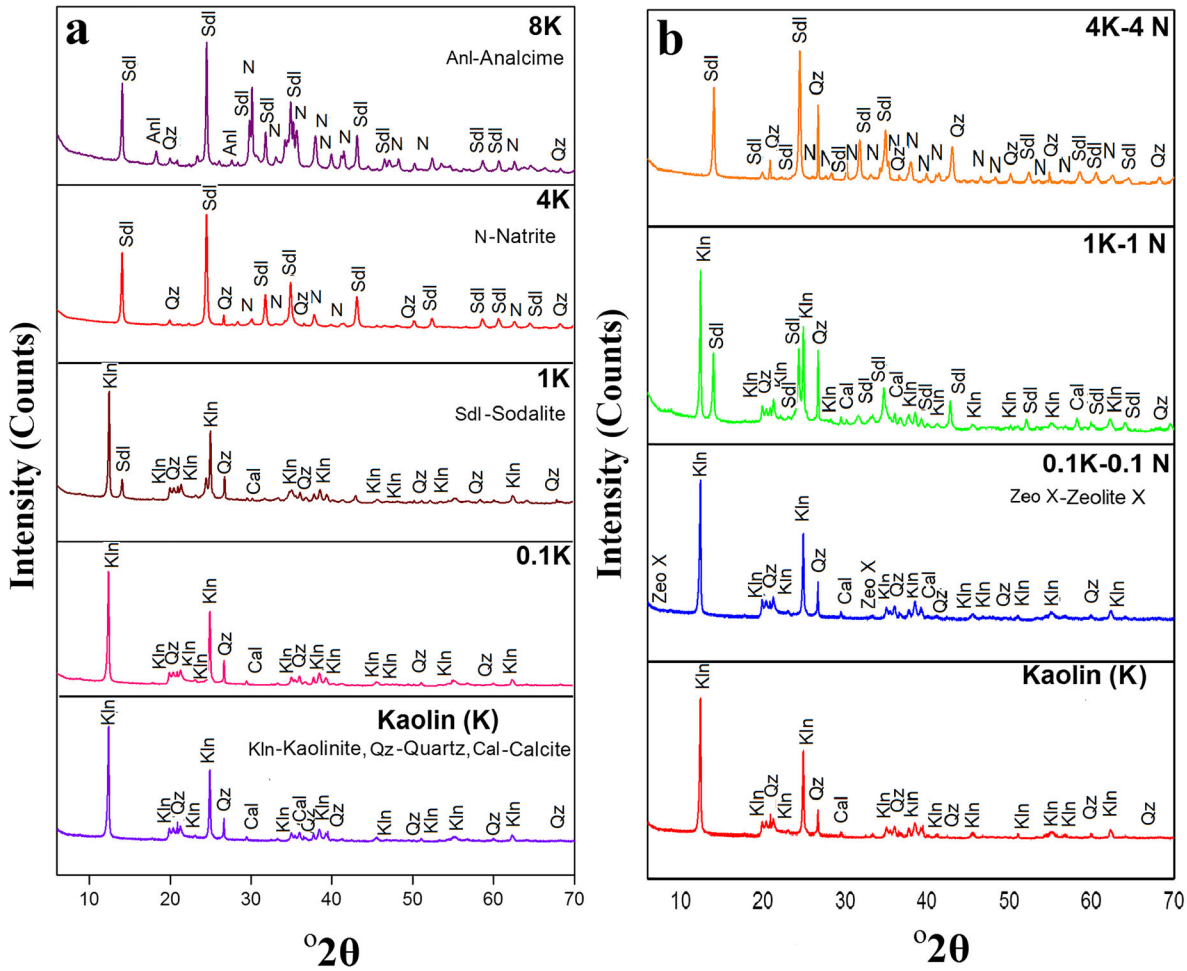

Fig. 9. XRD patterns of kaolin **a** before and **b** after swelling tests

third endothermic peak was followed by a negligible weight loss on the TG curve at ~977°C (Fig. 13a).

The DTA curves of the 0.1K and 1K samples (Fig. 13a) were similar to the untreated kaolin (K). The two samples were also characterized by three endothermic peaks. The first endothermic peak at 79°C (Fig. 13a) in 1K was due mainly to dehydration. The second at 501°C (Fig. 13a) with a mass loss of ~7% (Fig. 13b) was attributed to dehydroxylation of the mineral. This peak was a little broader and was shifted to a lower temperature in comparison to the peak in the K

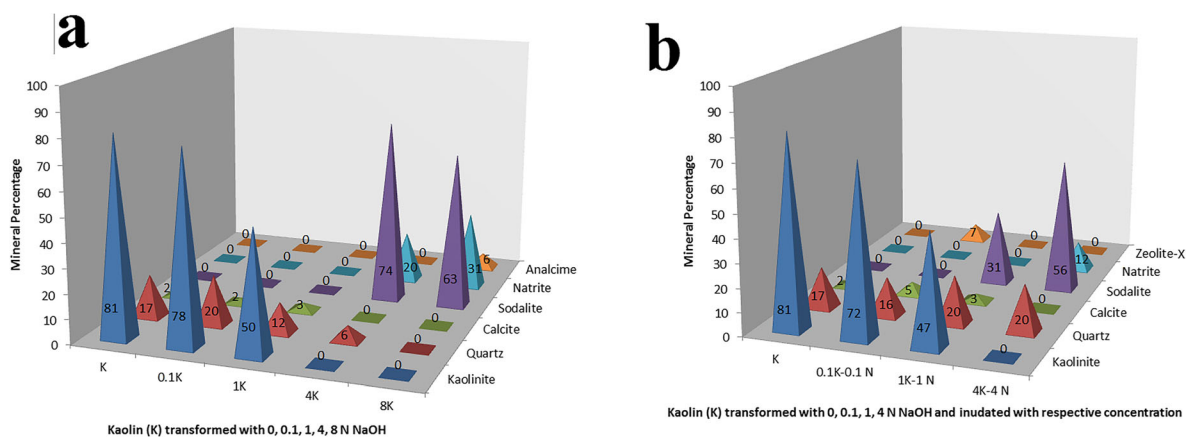

Fig. 10. Mineral quantification of transformed kaolin **a** before and **b** after swelling tests

https://doi.org/10.1007/s42860-020-00081-x Published online by Cambridge University Press

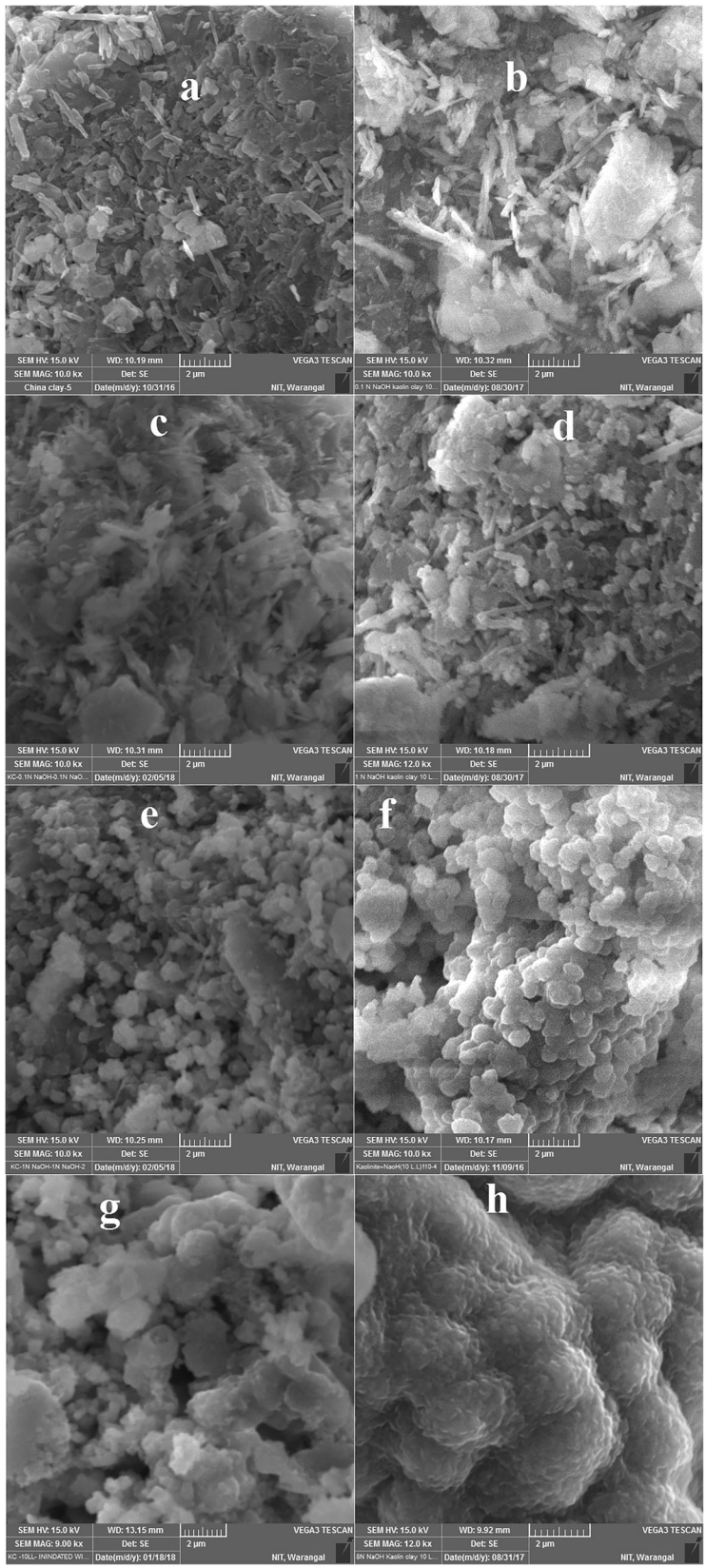

Fig. 11. SEM images of **a** kaolin, **b** 0.1K, **d** 1K, **f** 4K, and **h** 8K interacted with water; **c** 0.1K-0.1 N, **e** 1K-1 N, and **g** 4K-4 N

https://doi.org/10.1007/s42860-020-00081-x Published online by Cambridge University Press

Table 5. Assignments and infrared band positions of sample K and transformed K samples inundated with varying concentrations of NaOH solution

Sample no	Position (cm^{-1}) from previous studies	K	0.1K	1K	4K	8K	0.1K-0.1 N	1K-1 N	4K-4 N	Assignments
1	3696, 3621	3696, 3621	3694, 3619	3694, 3620	3638	------	3695, 3619	3695,3620	3637	-OH stretching
2	3670-56	3653,3669	3668	3652, 3668	-------	------	3668	3652	-------	Al–O–H stretching of inner surface hydroxyls
3	3445	3481	3453	3452	3432	3455	3465	3467	3458	Al–O–H stretching (physisorbed water)
4	2924	----	---	---	2924, 2494	------	------	------	------	C–H stretching
6	1632	1632	1639	1645	-------	1653	1638	1645	1654	-OH bending, hydration
7	1426	1426	1416	1455	1449	1432	----	1476,1414	1454,1409	CO_3 stretching of calcite
8	1032, 1008	1032,1008	1032	1031, 1007	978	983	1031	1006	979	Si -O stretching, in-plane/ Si–O–Si stretching (Frost et al. 2004)
9	913	913	912	912	------	------	912	913	-----	Al-OH bending
10	864				879	863	-----	-----	865	Carbonate ion vibrations (Blanco et al. 2011)
11	798	798	796	796	------	------	795	795	------	OH deformation linked to Al^{3-}
12	750-670	-----	755	752	708	735,707	754	-----	733,704	Presence of zeolites/ Si–O–Al str
13	696	696	697	695	------	686	695	694	687	Si–O stretching, out-of-plane
14		-----	------	------	665	664	------	660	662	*Alumino silicates
15	538	538	538	538	------	-----	538	538	------	*Fe–O, Fe_2O_3; Si–O–Al stretching
16	475-68	470	470	469	463	465	467	470	461	Si–O–Si bending
17	430	------	430	431	433	432	430	430	431	Si–O deformation

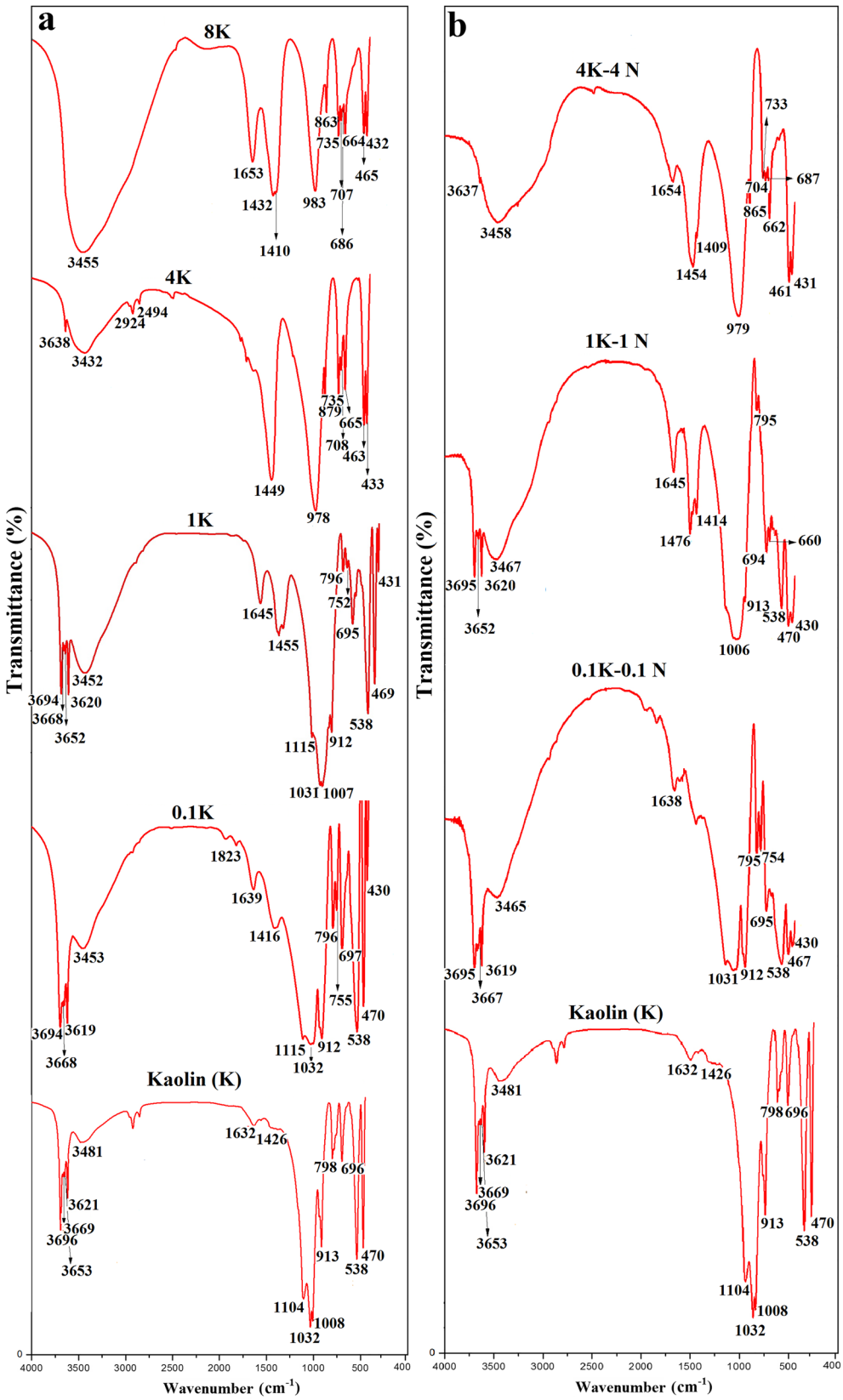

Fig. 12. FTIR spectra of **a** kaolin and **b** alkali-transformed kaolin interacted with various NaOH concentrations

https://doi.org/10.1007/s42860-020-00081-x Published online by Cambridge University Press

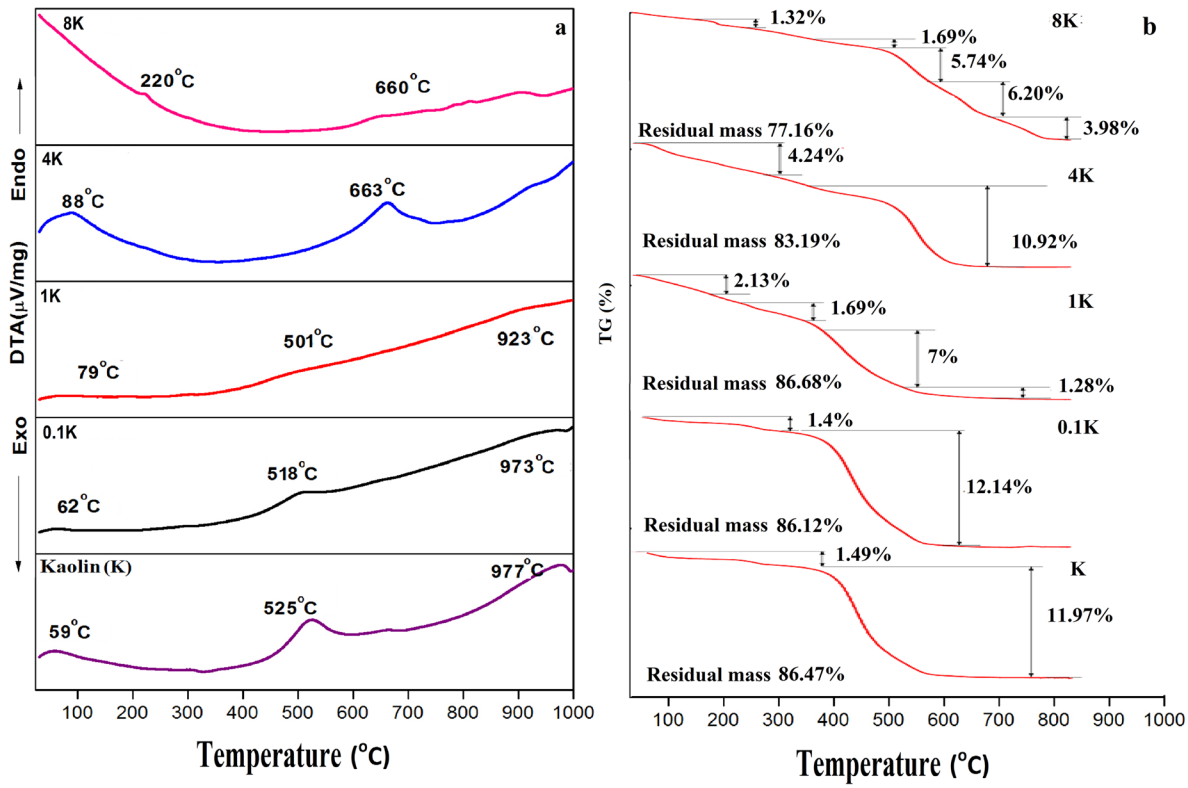

Fig. 13. **a** DTA and **b** TG curves of kaolin, reacted with various NaOH concentrations

specimen. This indicated that kaolinite was affected by the 1 N NaOH alkali solution treatment. Endothermic peaks at 973 and 923°C (Fig. 13a) in samples 0.1K and 1K corresponded to the transformation of kaolinite into more stable phases, and also to the decomposition of other minerals that were present, such as carbonates (Rocha and Klinowski 1990). Decomposition of calcite (calcium carbonate) as indicated by the absence of peaks in the XRD patterns of respective samples supports the above statement mentioned by Rocha and Klinowski (1990). An endothermic peak at 88°C was observed in sample 4K with a mass loss of ~4.24% (Fig. 13). This mass loss was due mainly to the escape of water molecules from zeolite cavities (Sruthi and Reddy 2017). Further, a sharp endothermic peak at 663°C (Fig. 13a) with a notable weight loss of 10.92% was due to decomposition of sodalite. The DTA curve of sample 8K exhibited an endothermic peak at 220°C (Fig. 13a) with a resultant mass loss of 1.32%, which may be attributed to the dehydration of analcime present in the sample. Koizumi (1953) and Milligan and Weiser (1937) mentioned that analcime dehydrates gradually between 200 and 400°C. Similar to sample 4K, in the 8K sample an endothermic peak at 660°C (Fig. 13a) indicated sodalite decomposition at higher temperatures. The endothermic peak that appeared between 450 and 650°C was due to the dehydroxylation of kaolinite (Moropoulou et al. 1995; Hajjaji et al. 2002; Palanivel and Rajesh 2011), but the absence of kaolinite highlighted its dissolution at higher concentrations, i.e. samples 4 N and 8 N NaOH.

The DTA curve of the 0.1K-0.1 N sample (Fig. 14a) was similar to the untreated kaolin. An endothermic peak at 635.4°C in 1K-1 N corresponded to sodalite decomposition. The endothermic peaks observed at 113 (1K-1 N) and 113°C (4K-4 N) were due mainly to the loss of water molecules from zeolite cavities (the presence of zeolites can be seen from XRD analysis; Fig. 9b).

DISCUSSION

Mechanism Involved in the Swelling Behavior of Red Earth Samples (Non-transformed and Transformed)

Swelling of ~1% for sample R in water (Fig. 1) was due to a lack of significant isomorphous substitution that led to a relatively small net negative charge and small cation exchange capacity. The cementitious nature of the iron oxides (Rao and Rao 1994; Sivapullaiah and Manju 2006) in sample R (shown in XRD analyses) bound the soil particles into coarse aggregates, which resulted in less swelling. The transformed red earth sample (0.1R) exhibited swelling of ~3% when inundated with water (Fig. 1a), however. The increase in swelling was due mainly to the presence of Na^+ ions. Sodium ions favor the formation of an opened edge-to-face (EF) association due to the dominant Coulombic attraction between faces and edges (Wang and Siu 2006a), which leads to a volume increase. Samples 1R and 4R inundated with water (1R-W and 4R-W) exhibited swelling of ~5% (Fig. 1b) and 8% (Fig. 1c), respectively. The increased swelling of 1R-W was due partly to fabric flocculation (as explained for 0.1R-W) and partly to new-

https://doi.org/10.1007/s42860-020-00081-x Published online by Cambridge University Press

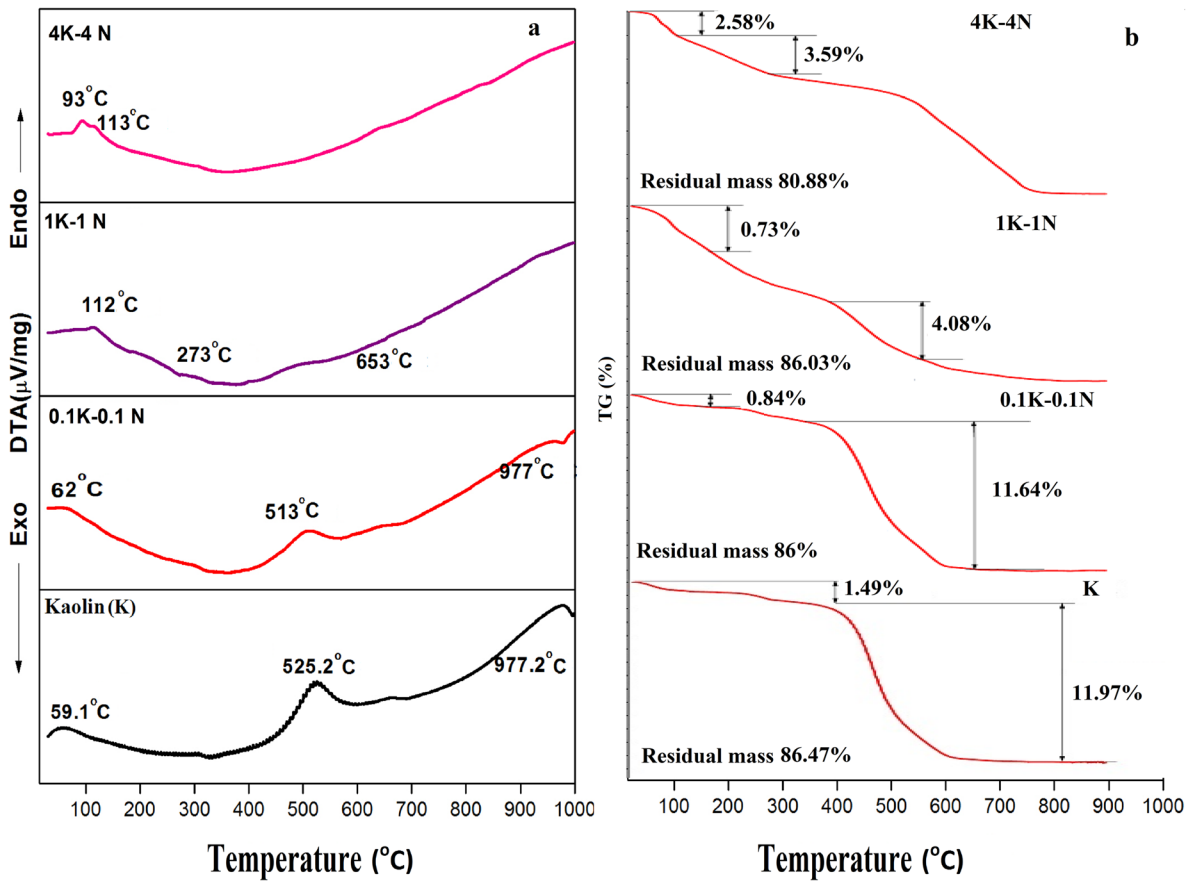

Fig. 14. **a** DTA and **b** TG curves of alkali-transformed kaolin samples, reacted with various NaOH concentrations

mineral formation (confirmed by XRD, Fig. 2). Whereas in 4R-W, increased swelling was due mainly to new-mineral formation (Fig. 2), Neogene minerals (sodalite, a zeolite) took place during transformation in 1R and 4R. The zeolites have open honeycomb structures with a negative charge (Sivapullaiah and Manju 2006). These zeolites are porous and host water molecules (Sand and Mumpton 1976); the sodalite imbibes water and eventually swells. Kranz et al. (1989), Heidug and Wong (1996), and Bish (2013) reported that zeolites exhibit expansion on hydration, supporting the swelling of alkali-transformed red earth due to the formation of zeolite minerals.

The observation made by Chavali et al. (2016) in their studies on non-transformed red earth samples inundated with various concentrations of alkali solution were considered to explain the swelling behavior of the transformed red earth samples inundated with the respective alkali solutions. Red earth samples, when inundated with 0.1N (R-0.1 N), 1N (R-1 N), and 4N (R-4 N) NaOH, exhibited maximum swellings of ~27% (Fig. 1a), 22% (Fig. 1b), and 22% (Fig. 1c), respectively. The variations in swelling behavior of the red earth samples inundated with alkali could be explained by three possible mechanisms (Kabanov et al. 1977): (1) dispersion of structure; (2) loss of iron oxide coatings; and (3) new-mineral formation. Further, the swelling is exhibited by phases that depend on the alkali concentration: Phase-I – swelling takes place mainly due to the dominant effects of pH and electrolytes; Phase-II – a relative stabilization period (i.e. transition zone with the absence of swelling) where reaction between soil particles and NaOH begins and continues to reach a certain value; Phase-III – swelling takes place mainly due to the formation of new minerals such as zeolites.

The swelling in 0.1R-0.1 N (Fig. 1a) was governed explicitly by mechanism 1 and the swelling pattern further confirmed that the swelling was due mainly to a pH effect (phase-I). Sample 0.1R-0.1 N exhibited less swelling (17%) than did R-0.1N (27%, Fig. 1a), however, due to a reduction in the phase-I swelling pattern. This reduction in Phase-I swelling was explained as follows: (1) during the transformation process (before the sample was subjected to swelling), partial dispersion of soil particles i.e. face-to-face association (Mitchell 1993), took place which did not occur during phase-I swelling; (2) the absence of mechanism 2 was due to the iron oxides (Fig. 2b) which do not add to phase-I swelling. Therefore, the 0.1R-0.1 N samples showed less tendency to swell compared to the R-0.1 N sample.

In sample 1R-1 N (Fig. 1b), the maximum swelling was ~14%, which was less than that observed for sample R-1 N (22%, Fig. 1b). The decrease in swelling was due to: (1) a reduction in the phase-I swelling, which was

https://doi.org/10.1007/s42860-020-00081-x Published online by Cambridge University Press

found to be even less than the phase-I swelling of 0.1R-0.1 N; and (2) the absence of mechanism 2. The reduction in Phase-I was due mainly to the accumulation of excess Na ions, which reflects the significance of the electrolyte effect. Mechanism 2, which deals with the dissolution of iron oxide that leads to swelling (Rao and Rao 1994), was absent because the dissolution of iron oxide occurred during transformations (Fig. 2a) and minimized the swelling in 1R-1 N. The relative stabilization period i.e. phase-II, which activated the soil for the next stage was completely absent (Fig. 1b) because the formation of new minerals was initiated during the transformation period. Therefore, the majority of swelling observed in 1R-1 N was mainly during phase-III, where the formation of new minerals initiated the swelling. The result indicated, therefore, that the swelling mechanism in transformed red earth i.e. 0.1R-0.1 N, was governed mainly by mechanism 1 and 1R-1 N was governed mainly by mechanisms 1 and 3. A minimum swelling of 7% was observed in sample 4R-4 N, which was much less than the swelling in R-4 N, i.e. 22% (Fig. 1c). Mechanisms 1, 2, and 3, which govern the swelling in R-4 N, took place during the transformation period and did not occur during the swelling of 4R-4 N. Complete reduction in the phase-I swelling pattern, absence of a stabilization period (phase-II), and minimal contribution of phase-III swelling led to decreased swelling in 4R-4 N. Also observed was that 4R-W (8%) exhibited more swelling compared to sample 4R-4 N (7%). At alkaline pH, double layer repulsion exists, which rendered the dispersed and deflocculated structure (Wang and Siu 2006a) subject to less swelling in 4R-4 N. The swollen phases in transformed soils 0.1R-0.1 N, 1R-1 N, and 4R-4 N could not be detected individually because the phases occurred concurrently.

Mechanism Involved in the Swelling Behavior of Kaolin Samples (Non-transformed and Transformed)

Similar to the red earth (R) sample, depending on the concentration of NaOH with which it interacted, kaolin (K) exhibited different mechanisms to induce swelling. In kaolin, mechanisms 1 and 3 are similar to red earth, whereas mechanism 2 was due to leaching of calcium carbonate instead of iron oxide in red earth. Like the red earth sample, the swelling induced by water in the alkali-transformed kaolin can be explained as follows: (1) in 0.1K-W, mostly due to fabric flocculation; (2) in 1K-W, partly due to fabric flocculation and partly to new-mineral formation; and (3) in 4K-W, mostly due to the formation of new minerals.

The increase in swelling at higher NaOH concentrations when inundated with water (1K-W and 4K-W) was due mainly to the formation of new minerals, i.e. sodalites (zeolite group minerals). Published research (Kranz et al. 1989; Heidug and Wong 1996; Bish 2013) supports the observed uncharacteristic swelling of alkali-transformed kaolin when inundated with water due to the formation of zeolite minerals.

The kaolin sample (0.1K-0.1 N) exhibited swelling of ~11%, which was less than the swelling of K-0.1 N (16%, Fig. 8a). This decrease in swelling was due mainly to the reduction in phase-1 swelling. This reduction in phase-I was due to: (1) the effects on particle orientation (mechanism 1), which was initiated during the transformation period and (2) the absence of mechanism 2 (i.e. dissolution of calcite, which induced swelling) because the calcite remained (XRD patterns of 0.1K (Fig. 9a) and 0.1K-0.1 N (Fig. 9b)). The relative stabilization (phase-II) initiated the next stage of new-mineral formation and phase-III highlighted the formation of new minerals, which were major contributors to the induced swell in 0.1K-0.1 N, which was not observed in sample K-0.1 N.

The 1K-1 N sample exhibited swelling of 8%, which was less than the swelling observed for K-1 N (12%, Fig. 8b). Mechanism 2, which deals with the dissolution of calcite, was absent because calcite remained (XRD patterns of 1K (Fig. 9a) and 1K-1 N (Fig. 9b)) and the relative stabilization period (transition), i.e. phase-II, was completely absent because the formation of new minerals was initiated during transformation. New-mineral formation was governed by mechanism 3 and enhanced phase-III swelling. The 4K-4 N sample exhibited 7% swelling, which was much less than the swelling exhibited by K-4 N (22%) (Fig. 8c). This difference in swelling was mainly attributed to the absence of mechanisms 1 and 2, which minimized phase-I swelling and the absence of phase II swelling. The mechanism 3-enhanced phase-III swelling was trivial because the formation of new minerals commenced during transformations. New-mineral formation (Fig. 9) increased compared to K-4 N but this did not enhance swelling. 4K-W (11%) also exhibited more swelling than 4K-4 N (8%). The interparticle forces and associated fabric formations were responsible for the decreased swelling in 4K-4 N. Double layer repulsion led to a dispersed/deflocculated structure, which tended to form denser soil packing in the sediment (Wang and Siu 2006a) and resulted in less swelling. Phases of swelling were not identified individually when alkali-transformed soils were inundated with water and in samples 0.1 N, 1 N, and 4 N NaOH because the swelling phases took place concurrently. This was due mainly to the transformations that had occurred in the samples prior to inundation.

From the above discussion, the swelling observed in transformed clays was less than that observed in non-transformed clays and was also inversely proportional to the alkali concentration of pore fluid. Higher alkali concentrations of pore fluid produced less swelling.

CONCLUSIONS

When concentrated alkali is released accidentally and enters moist ground, it spreads spatially, and is diluted to produce varying levels of contamination. Depending on the alkali concentration and the exposure period, soils are transformed to various degrees. In studying the swelling behavior of such transformed soils when subjected to various pore fluids, one must tackle the effects of the contamination. To mimic field contamination conditions and to understand the behavior of such soils, swelling studies were carried out in the laboratory on kaolinitic clays that were transformed using inundating

https://doi.org/10.1007/s42860-020-00081-x Published online by Cambridge University Press

fluids of various aqueous NaOH concentrations. The conclusions drawn from the results obtained are as follows:

- For a given volume of interacting solution, the degree of transformation of kaolinitic clays (i.e. the extent of the changes in mineralogy and microstructure) depended largely on the concentration of the alkali solution.
- Swelling in water increased as the degree of alkali transformation increased. Particle orientation and the extent of mineralogical changes were the key factors that enhanced swelling.
- Upon interaction with alkali, regardless of concentration, the swelling of non-transformed (untreated) kaolinitic clays was affected adversely. Particle orientation, leaching of secondary minerals, and the extent of mineralogical changes are the key factors that enhance swelling.
- Swelling in transformed (treated) kaolinitic clays decreased with increase in the concentration of interacting alkali solution. Leaching of secondary minerals and the magnitude of mineralogical changes during the transformation period are the key factors that inhibit swelling.

ACKNOWLEDGMENTS

The authors gratefully acknowledge the Centre for Automation and Instrumentation (CAI) and the Center for Advanced Materials (CAM) and Department of Chemistry, National Institute of Technology, Warangal, India, for providing facilities to carry out the XRD, SEM, and TG-DTA analyses.

Compliance with Ethical Standards

Conflict of Interest

On behalf of all authors, the corresponding author states that there is no conflict of interest

REFERENCES

Akokelar, D., Chasee, A., & Howe, R. F. (1997). The transformation of kaolin to low silica X zeolite. *Zeolites, 19*, 359–365.

Alshaaer, M. (2013). Two-phase geo polymerization of kaolinite-based geo polymer. *Applied Clay Science, 86*, 162–168.

Amadori, M.L., Pallante, P., Fermo, P., Emami, M.A., Chaverdi, A.A., Callieri, P., & Matin, E. (2018). Advances in Achaemenid brick manufacturing technology: Evidence from the monumental gate at Tol-e Ajori (Fars, Iran). *Applied Clay Science*, 152, 131–142.

Ayoob, N. F., Mohd Juoi, J., Rosli, Z. M., & Rosli, N. R. (2011). Characterisation and properties of sintered glass-ceramics produced from recycling glass by using pressure-less method. In: *Key Engineering Materials*, *471–472*, 933–938. Trans Tech Publications Ltd.

Ball, M. C., Snelling, C. M., Strachan, A. N., & Strachan, R. M. (1986). Thermal decomposition of solid sodium bicarbonate. *Journal of the Chemical Society, Faraday Transactions 1: Physical Chemistry in Condensed Phases, 82*, 3709–3715.

Barnes, M. C., Addai-Mensah, J., & Gerso, A. R. (1999). A methodology for quantifying sodalite and cancrinite phase mixtures and the kinetics of the sodalite to cancrinite phase transformation. *Microporous Mesoporous Materials, 31*, 303–319.

Barrer, R. M. (1982). *Hydrothermal Chemistry of Zeolites*. London: Academic Press.

Bish, D. L. (2013). Parallels and distinctions between clay minerals and zeolites. In: *Handbook of Clay Science* (F. Bergaya and G. Lagaly, editors). Developments in Clay Science, 5, pp. 783–800.

Blanco, J. D. R., Shaw, S., & Benning, L. G. (2011). The kinetics and mechanisms of amorphous calcium carbonate (ACC) crystallization to calcite, via vaterite. *Nanoscale, 3*, 265–271.

Boussen, S., Sghaier, D., Chaabani, F., Jamoussi, B., Messaoud, S. B., & Bennour. (2015). The rheological, mineralogical and chemical characteristic of the original and the Na_2CO_3 – activated Tunisian swelling clay (Aleg formation) and their utilization as drilling mud. *Applied Clay Science, 118*, 344–353.

Chavali, R. V. P., Vindula, S. K., Reddy, H. P. P., Ambili, B., & Rakesh Pillai, J. (2016). Swelling behavior of kaolinitic clays contaminated with alkali solutions: a micro-level study. *Applied Clay Science, 135*, 575–582.

Chermak, J. A. (1992). Low temperature experimental investigation of the effect of high pH NaOH solutions on the Opalinus shale, Switzerland. *Clay and Clay Minerals, 40*, 650–658.

Cuadros, J., & Linares, J. (1996). Experimental kinetic study of the smectite-to-illite transformation. *Geochimica et Cosmochimica Acta, 60*, 439–453.

Demortier, A., Gobeltz, N., Lelieur, J. P., & Duhayon, C. (1999). Infrared evidence for the formation of an intermediate compound during the synthesis of zeolite Na-A from metakaolin. *International Journal of Inorganic Materials, 1*, 129–134.

Diko, M., Ekosse, G., & Ogola, J. (2016). Fourier transform infrared spectroscopy and thermal analyses of kaolinitic clays from South Africa and Cameroon. *Acta Geodynamica et Geomaterialia, 13*, 149–158.

Elert, K., Sebastian, E., Valverde, I., & Rodriguez-Navarro, C. (2008). Alkaline treatment of clay minerals from the Alhambra formation: implications for the conservation of earthen architecture. *Applied Clay Science, 39*, 122–132.

Elert, K., Pardo, E. S., & Rodriguez-Navarro, C. (2015). Influence of organic matter on the reactivity of clay minerals in highly alkaline environments. *Applied Clay Science, 111*, 2–36.

Esfandian, H., Samadi-Maybodi, A., Parvini, M., & Khoshandam, B. (2016). Development of a novel method for the removal of diazinon pesticide from aqueous solution and modeling by artificial neural networks (ANN). *Journal of Industrial and Engineering Chemistry, 35*, 295–308.

Farmer, V. C. (1974). *The Infrared Spectra of Minerals*. London: Mineralogical Society.

Frost, R. L., Horvath, E., Mako, E., & Kristof, J. (2004). Modification of low- and high-defect kaolinite surfaces: implications for kaolinite mineral processing. *Journal of Colloid and Interface Science, 270*, 337–346.

Garvie, R. C., & Nicholson, P. S. (1972). Phase analysis in zirconia systems. *Journal of the American Ceramic Society, 55*, 303–305.

Hajjaji, M., Kacim, S., & Boulmane, M. (2002). Mineralogy and firing characteristics of a clay from the valley of Ourika (Morocco). *Applied Clay Science, 21*, 203–212.

Heidug, W. K., & Wong, S. W. (1996). Hydration swelling of water absorbing rocks: A constitutive model. *International Journal for Numerical and Analytical Methods in Geomechanics, 20*, 403–430.

Ibrahim, K. (2004). Mineralogy and chemistry of natrolite from Jordan. *Clay Minerals, 39*, 47–55.

Jiang, T., Li, G., Qui, G., Fan, X., & Huang, Z. (2008). Thermal activation and alkali dissolution of silicon from illite. *Applied Clay Science, 40*, 81–89.

Johnson, E. B. G., & Arshad, S. E. (2014). Hydrothermally synthesized zeolites based on kaolinite: a review. *Applied Clay Science, 97–98*, 215–221.

Jozefaciuk, G. (2002). Effect of acid and alkali treatments on surface charge properties of selected minerals. *Clays and Clay Minerals, 50*, 647–656.

Kabanov, V. M., Lebedeva, G. A., Finkel'shtein, L. I., Tkachenko, G. P., & Shenin, O. S. (1977). Swelling of soils due to wetting with

alkali solutions. *Soil Mechanics and Foundation Engineering, 14*, 338–339.

Kamseu, E., Lancellotti, I., Sglavo, M. V., Modolo, L., & Leonelli, C. (2016). Design of inorganic polymer mortar from ferricalsialic and calsialic slags for indoor humidity control. *Materials, 9*, 410–428.

Khajavi, S., Kapteijn, F., & Jansen, J. C. (2007). Synthesis of thin defect-free hydroxy sodalite membranes: New candidate for activated water permeation. *Journal of Membrane Science, 299*, 63–72.

Koizumi, M. (1953). The differential thermal analysis curves and the dehydration curves of zeolites (studies on water in minerals, part 1). *Mineralogical Journal, 1*, 36–47.

Kranz, R. L., Bish, D. L., & Blacic, J. D. (1989). Hydration and dehydration of zeolitic tuff from Yucca Mountain, Nevada. *Geophysical Research Letters, 16*, 1113–1116.

Liu, Y., & Naidu, R. (2014). Hidden values in bauxite residue (red mud): recovery of metals. *Waste Management, 34*, 2662–2673.

Madani, A., Aznar, A., Sanz, J., & Serratosa, J. M. (1990). ^{29}Si and ^{27}Al NMR study of zeolite formation from alkali-leached kaolinites influence of thermal preactivation. *The Journal of Chemical Physics, 94*, 760–765.

Maltsev, A. V. (1998). Theoretical and experimental investigations of the effect of aggressive wetting on various types of bed soils. *Soil Mechanics and Foundation Engineering, 35*, 83–86.

Mazaheri, M., Simchi, A., & Golestani-Fard, F. (2008). Densification and grain growth of nanocrystalline 3Y-TZP during two-step sintering. *Journal of the European Ceramic Society, 28*, 2933–2939.

Milligan, W. O., & Weiser, H. B. (1937). The mechanism of dehydration of zeolites. *The Journal of Physical Chemistry, 41*, 1029–1040.

Mitchell, J. K. (1993). *Fundamentals of Soil Behavior* (2nd ed.). New York: Wiley.

Mohnot, S.M., Bae, J.H., & Foley, W.L. (1987). A study of alkali/mineral reactions. *SPE Reservoir Evaluation & Engineering,* 653–663.

Moropoulou, A., Bakolas, A., & Bisbikou, K. (1995). Thermal analysis as a method of characterizing ancient ceramic technologies. *Thermochimica Acta, 2570*, 743–753.

Mulyukov, E. I. (2008). Alkaline swelling and consequences of alkalization of clayey bed soils. *Soil Mechanics and Foundation Engineering, 45*, 182–185.

Ogbaji, P. O., Li, J., Xue, X., Shahrajabian, M. H., & Eneji, A. E. (2018). Mineralogical and textural characteristics of soils of Hancheng and Shannxi Province, China. *Communications in Soil Science and Plant Analysis, 49*, 286–290.

Onojake, M. C., & Frank, O. (2013). Assessment of heavy metals in a soil contaminated by oil spill: a case study in Nigeria. *Chemistry and Ecology, 29*, 246–254.

Palanivel, R., & Rajesh Kumar, U. (2011). The mineralogical and fabric analysis of ancient pottery artifacts. *Cerâmica, 57*, 56–62.

Popescu, S. C., Thomson, S., & Howe, R. F. (2001). Microspectroscopic studies of template interactions in and AlPO4-5 SAPO-5 crystals. *Physical Chemistry Chemical Physics, 3*, 111–118.

Puppala, A. J., Napat, I., & Rajan, K. V. (2005). Experimental studies on ettringite-induced heaving in soils. *Journal of Geotechnical and Geoenvironmental Engineering, 131*, 325–337.

Rao, S. M., & Rao, K. S. S. (1994). Ground heave from caustic soda solution spillage: a case study. *Soils and Foundations, 34*(*2*), 13–18.

Reddy, P. H. P., & Sivapullaiah, P. V. (2010a). Effect of alkali solutions on the swell behavior of soils with different mineralogy. *GeoFlorida 2010*: *Advances in Analysis, Modeling and Design*. *Geotechnical Special Publication, 199*, 2692–2701.

Reddy, P.H.P. & Sivapullaiah, P.V. (2010b). Mineralogical and Morphological Changes with Alkali Treatment of Soils. *Indian Geotechnical Conference – 2010, GEOtrendz December* 16–18, 2010, IGS Mumbai Chapter & IIT Bombay

Reddy, H. P., Prasad, C. R. V., & Pillai, R. J. (2017). Swelling of natural soil subjected to acidic and alkaline contamination. *Periodica Polytechnica Civil Engineering, 61*, 611–620.

Ren, T. Z., Yuan, Z. Y., & Su, B. L. (2003). Surfactant-assisted preparation of hollow microspheres of mesoporous TiO_2. *Chemical Physics Letters, 374*, 170–175.

Rocha, J., & Klinowski, J. (1990). ^{29}Si and ^{27}Al magic-angle-spinning NMR studies of the thermal transformation of kaolinite. *Physics and Chemistry of Minerals, 17*, 179–186.

Russell, A. (1924). Topaz from Cornwall, with an account of its localities. *Mineralogical Magazine, 20*, 221–236.

Samal, S., Ray, A. K., & Bandopadhyay, A. (2013). Proposal for resources, utilization and processes of red mud in India – a review. *International Journal of Mineral Processing, 118*, 43–55.

Sand, L.B. & Mumpton, F.A. (1976). Natural zeolites occurrence, properties, use, a selection of papers presented at Zeolite, 76, *an International Conference on the occurrence, Properties and Utilization of Natural Zeolite,* Tucson, Arizona, USA, pp. 135–137.

Schnabel, K. H., Finger, G., Kornatowski, J., Loffler, E., Peuker, C., & Pilz, W. (1997). Decomposition of template in SAPO-5 and AlPO4-5 molecular sieves studied by IR and Raman spectroscopy. *Microporous Materials, 11*, 293–302.

Shekhtman, L. M., Baranov, V. T., & Nesterenko, G. F. (1995). Building deformations caused by the leakage of chemical reagents. *Soil Mechanics and Foundation Engineering, 32*, 32–36.

Sivapullaiah, P. V., & Manju, M. (2006). Effect of zeolitization on the volume-change behavior of kaolinitic soils. *Canadian Geotechnical Journal., 43*, 969–978.

Sivapullaiah, P. V., & Reddy, P. H. P. (2009). Fly ash to control alkali induced volume changes in soils. *Ground Improvement, 162*, 167–173.

Sivapullaiah, P. V., Sankara, G., & Allam, M. M. (2010). Mineralogical changes and geotechnical properties of an expansive soil interacted with caustic solution. *Environmental Earth Sciences, 60*, 1189–1199.

Smith, P. (2009). The processing of high silica bauxites – review of existing and potential processes. *Hydrometallurgy, 98*, 162–176.

Sokolovich, V. E., & Troitskii, G. M. (1976). Heaving of a sand base as a consequence of the development of secondary crystal hydrate formations. *Soil Mechanics and Foundation Engineering, 13*, 376–378.

Sruthi, P. L., & Reddy, H. P. P. (2017). Characterization of kaolinitic clays subjected to alkali contamination. *Applied Clay Science, 146*, 535–547.

Standard Methods for the Examination of Water and Wastewater, (23rd Ed.) (2017). *American Public Health Association, American Water Works Association, Water Environment Federation*.

Taubald, H., Bauer, A., SchAafer, T., Satir, M., & Kim, J. I. (2000). Experimental investigation of the effect of high-pH solutions on the Opalinus shale and the Hammerschmiede smectite. *Clay Minerals, 35*, 515–524.

Vaiciukyniene, D., Baltakys, K., & Kantautas, A. (2009). Hydrosodalite ion exchange in saturated $Ca(OH)_2$ solution. *Materials Science – Poland, 27*, 417–426.

Wang, Z. (2003). Fate and identification of spilled oils and petroleum products in the environment by GC-MS and GC-FID. *Energy Sources, 25*, 491–508.

Wang, Y., & Siu, W. (2006a). Structure characteristics and mechanical properties of kaolinite soils. 1. Surface charges and structural characterizations. *Canadian Geotechnical Journal, 43*, 587–600.

Wang, Y., & Siu, W. (2006b). Structure characteristics and mechanical properties of kaolinite soils. 1. Effects of structure on mechanical properties. *Canadian Geotechnical Journal, 43*, 601–617.

Zubkova, N. V., Pushcharovsky, D. Y., Ivaldi, G., Ferraris, G., Pekov, I. V., & Chukanov, N. V. (2002). Crystal structure of natrite, γ-Na_2CO_3. *Neues Jahrbuch für Mineralogie-Monatshefte, 2002*(*2*), 85–96.

(Received 5 October 2019; revised 15 May 2020 AE: William F. Jaynes)